2012

Force sensing of an asymmetric dielectric barrier discharge using mechanical resonators

Mark Dawson Emanuel

Department:

FORCE SENSING OF AN ASYMMETRIC DIELECTRIC BARRIER DISCHARGE USING MECHANICAL RESONATORS

by

MARK DAWSON EMANUEL

A THESIS

Presented to the Faculty of the Graduate School of the

MISSOURI UNIVERSITY OF SCIENCE AND TECHNOLOGY

In Partial Fulfillment of the Requirements for the Degree

MASTER OF SCIENCE IN MECHANICAL ENGINEERING

2012

Approved by

Douglas A. Bristow, Co-advisor
Joshua L. Rovey, Co-advisor
Daniel C. Stutts

ABSTRACT

Dielectric barrier discharge (DBD) plasma actuators are of great interest in flow control research and application. DBD plasma actuators are low-cost, lightweight, high voltage devices that have the capability of generating small amounts of thrust on the order of a few tenths of a gram. The thrust is created by rapidly pulsing plasma discharges which correlate to the frequency of the applied alternating current waveform, in the low kilohertz range.

Plasma actuators experience a reactant force generated by the pulsed plasma charging and then expelling air away from the charged surface. This force fluctuates with time as the plasma is created and then extinguished, twice per cycle for a sine wave input. This research uses tuned harmonic resonators to amplify the motion of a plasma actuator, which for a 10 gram actuator is less than one nanometer in distance per cycle. Reflective mirrored stainless steel double-clamped beams are used in conjunction with a laser interferometer system capable of resolving 0.0791 nanometers at a bandwidth of 50MHz. Resonators designed for this application provide motion amplification of 100 times or greater.

The total system, although highly sensitive to outside motions, is capable of detecting nanometer and sub-nanometer motion of a plasma actuator running at nominal voltages of 6.5-9.3kV and a frequency of 3kHz. Periodic displacements, and the forces that cause them, are measured.

ACKNOWLEDGEMENTS

I would like to thank my advisors, Dr. Douglas Bristow and Dr. Joshua Rovey, for demonstrating more patience with me than I could have possibly expected. Their insights into the subject matter at hand, their ability to guide me through the arduous process known as academic research, and their willingness to overlook my nefarious puns made two years of graduate school palatable, if not occasionally enjoyable.

My colleagues in the Precision Motion Control Lab, particularly Patrick, Muthu, Tong, Santosh, Ali, and Emily, are worthy of praise for the long nights of quality scientific conversation and social activities outside of the office. My colleagues in the Aerospace Plasma Lab, including Timothy, Steve, Alex, Warner, Ryan, Andrew, and Jing, deserve thanks for answering my multitude of questions and putting up with my incessant complaining.

I am forever indebted to the assistance of Dr. Lokesh Dharani, whose encouragement and advisement set my graduate career in motion well ahead of landing on campus; Dr. Daniel Stutts for agreeing to be on my committee; Chancellors John Carney and Cheryl Schrader for picking up the tuition tab; the department secretaries Kathy, Kimber, and Elaine for all their assistance; the "Tech Shop Boys" Bob (enjoy your retirement!), Joe, George, and Randall for making good work of my awful hand sketches; to all my ME240 students for their youthful extravagance; and to my boss in the instrumentation lab, Mitch Cottrell, who gave me the best TA job I could have asked for.

To those family, friends, and co-workers whose names do not appear here, your support- even if I didn't acknowledge it then- is only left out on paper, and not in my heart. Thank you all.

TABLE OF CONTENTS

LIST OF ILLUSTRATIONS

LIST OF TABLES

1. INTRODUCTION

1.1. DESCRIPTION OF DIELECTRIC BARRIER DISCHARGE PLASMA ACTUATORS

Plasma actuators of the dielectric barrier discharge (DBD) variety are simplistic in their nature. A graphic portraying the physical configuration of a DBD is given in Figure 1.1. The mechanism of action is straightforward. A grounded buried conductor is separated from an exposed high voltage conductor by a small dielectric layer. A potential difference applied between electrodes is sufficient to break down the air and form a layer of plasma at the edge of the exposed electrode. Somewhat unique to the general field of plasma study is that the DBD can operate at atmospheric pressures. Ambient air molecules are ionized and then accelerated away from the barrier creating a small body force on the actuator (or conversely the air) when excited by the plasma discharge.

Construction of a plasma actuator can be quite variable with a myriad of different conductors, dielectrics, and substrates. Many actuators used in research applications are built with one or more layers of Kapton tape as a dielectric insulating two layers of copper tape. Thinly constructed ceramic such as Macor can also be used as a dielectric barrier. Substrate materials are kept rigid and light in weight, with Styrofoam common due to affordability and availability. If ceramics are used as the dielectric, a rigid substrate is not necessary.

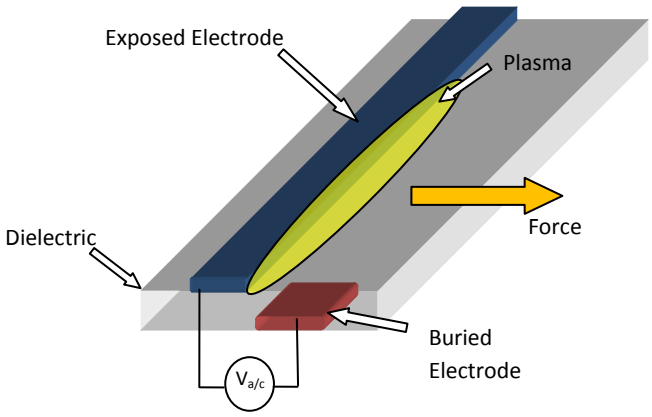

Figure 1.1. DBD Plasma Actuator Schematic

Plasma generation occurs in two phases: during an upstroke in applied voltage and during a downstroke. Plasma power is derived from measured current, normally in milliamps, whereas applied voltage is normally measured in kilovolts. High voltage is necessary to break down the insulation of the air around the dielectric in order to generate plasma. Through experimental research, it is well known that plasma current is highest during the maximum upstroke rate of driving voltage, and that plasma current experiences a secondary peak during the maximum downstroke rate. Consequently, plasma is generated twice when excited by a sinusoidal voltage waveform. Other waveforms, like a saw or square wave, have significant effect on plasma generation and have been investigated by Benard and Moreau [1].

Plasma actuator application has been extensively studied in recent years. The most frequently idealized application is for flow control devices where precise, small scale flow modification is beneficial. Jet turbine flow stabilization [2], stall detection [3], and improving angle-of-attack dynamics [4,5] are among the potential uses for DBD actuators in the aerodynamic field. Boundary layer separation control [6] is of great

interest for application in aerodynamic design. Whether aerodynamic application is feasible in reality remains to be seen, as the power requirements for DBD plasma actuators are fairly low, they do require additional electrical equipment that only serve to add mass to aircraft systems where low mass is a necessity (such as in pilotless aircraft drones). Plasma actuators can also be used for atmospheric ozone generation and may be useful for sterilization of biological contaminants [7].

1.2. THE NEED FOR TIME-RESOLVED THRUST MEASUREMENTS

Thus far, plasma actuator force production is a matter of some contention in the research field. What is known is that the plasma actuator creates a small amount of constant thrust when it is generating plasma (a "DC" force). What is less clear, however, are the minute changes in force as the driving alternating current signal impacts plasma generation (an "AC", or time-varying, force).

The reasoning for determining time-resolved thrust is that, once known, plasma actuator construction can be more fully optimized. For example, construction materials or actuator dimensions can be modified in order to maximize the time-varying thrust, shape the intensity of the thrust, or smooth the thrust. The ability to know the time-resolved thrust will add a great deal to the overall understanding of the plasma actuator system and how to design an actuator to meet criteria set for an end purpose.

Knowing the time-resolved thrust of a plasma actuator could also yield greater insight into plasma physics. Modeling of plasmas using either a kinetic or fluid scheme could be well served to fully diagnose DBD plasma behavior using time-resolved thrust data as an input variable. Current modeling is heavily based on indirect measurements

from camera-based visual images, which does not numerically characterize the time-resolved thrust. Incorporation of time-resolved force measurements can either validate existing models or help to improve them.

Highly resolved temporal force measurement can potentially yield great advances in plasma actuator optimization. Although constant DC force has been well-studied, and effects from high altitudes, different voltage waveforms, and construction parameters have been uncovered, the ability to finely resolve force measurements with time will greatly improve insight into the physics behind the plasma.

2. LITERATURE REVIEW

Plasma generation has been studied for much of the past 100 years, dating back to Langmuir's early work in the 1920s. Early applications of plasma were focused on atmospheric ozone generation. The field of DBD study began in 1998 with a conference paper by Roth who first discovered that airflow could be induced by DBD plasma [8]. Applications of the discovery began in earnest in the early 2000s when plasma actuation as a flow control device was published by Corke and Matlis [9]. Investigators found that a thin layer of plasma using a single dielectric layer could impart velocity onto air molecules. One particular aspect that interested researchers is that DBD plasma is non-thermal and can be used at high (atmospheric) pressures, unlike other forms of plasma which are useful in low pressure applications as a means of generating thrust. DBD actuators had the benefit of being light in weight, using no moving parts, and could be mated to a wide variety of surfaces [10]. It was quickly determined that atmospheric pressure plasma actuators generate thrust of their own.

2.1. DC THRUST MEASUREMENTS

As plasma is generated along the length of the actuator, air is excited and accelerated away from and along the surface of actuation. A reactant force is imparted on the actuator which causes the actuator to produce some amount of thrust. Constant force measurements have been well established in research [11-14]. Force is generally a few millinewtons (or tenths of a gram) and depends on a number of factors, including thickness of the dielectric, pressure, and power levels. The general approach used to measuring the DC force consists of an actuator mounted vertically attached to a beam

with a counterweight on the end. The beam is allowed to pivot and the center of gravity is located at the pivot, making the actuator essentially weightless. As plasma is generated, the actuator pushes against a measuring scale in order to determine the amount of force.

The measurement using a scale is considered a DC thrust since the amount of force, although rapidly changing with plasma pulses, cannot be resolved temporally. In other words, much of the existing literature is measuring a time-averaged force and not a time-resolved force.

2.2. TIME-RESOLVED THRUST MEASUREMENTS

Plasma actuators are driven by high voltage, high frequency alternating current, creating a non-constant plasma force. In fact, previous work has shown that for every alternating current cycle, plasma is created twice: once during the forward stroke and once during the backward stroke [13]. Whereas studies of optimizing plasma (and, thus, force) generation are ongoing, there is a need to clarify how the plasma body force varies with respect to time. Other previous works have involved using optical and mechanical methods to identify the time-varying force [15,16]. Specifically, dual-mode time-resolved plasma forces involving a PUSH-push and push-pull force have been investigated.

Original works by Baird [17] have utilized acoustic derivation to determine a PUSH-push force, and have recently been investigated by Font [18] using a resonant actuator. Optical derivation of a push-pull force has been measured by Porter using sensitive high-speed cameras to capture the optics generated by the plasma [19]. The

challenge here is that the inertia of the actuator body acts like a filter, eliminating the higher frequency harmonics of the plasma force.

Optical measurements using high-speed cameras (a process known as particle image velocimetry, or PIV) are a commonly used method to determine force [20]. Issues arise with using existing methods such as PIV and the commonly used weighing scale. A few that Durscher and Roy [20] point out include:

1) Self-induced drag on the scale plate from the accelerated air coming from the actuator,
2) Control volumes (the sealed box in which the actuators are mounted and excited) can vary in size depending on the experiment and can impact force production,
3) The gas chemistry changes with time as oxygen is converted into ozone in a control volume, impacting force values,
4) Pitot tubes, used to validate PIV measurements, cannot capture all of the moving air being pushed away from the actuator.

PIV measurements also are intrinsically indirect, relying on visual inferences to determine force values. Still, the method is widely used [21-23] and serves a purpose to gather force measurements that are in agreement with DC thrust measurements. As confirmed in Figure 2.1, it is well known that the DC (average) force of DBD plasma actuators is on the order of tenths of a gram (millinewtons) per foot of actuator [14].

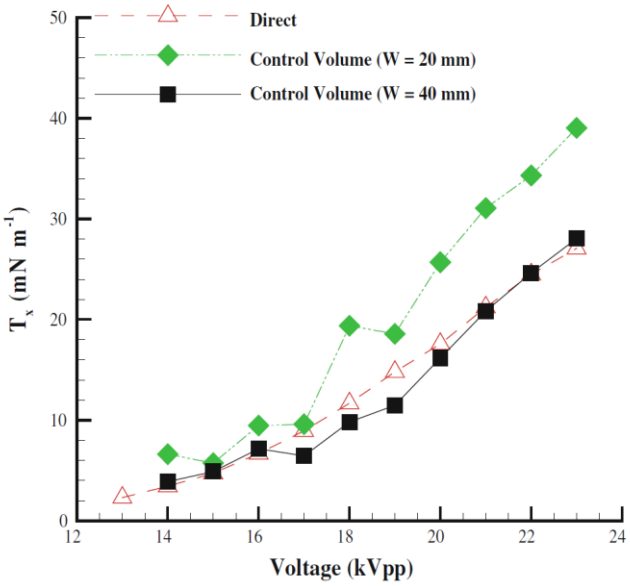

Figure 2.1. DC thrust measurements compared with PIV measurements [20]

Although PIV measurements can agree with DC thrust measurements, fine time-resolved force measurements are more difficult to validate. One recent investigation was able to yield time-resolved measurements and compared the force to the timing of voltage and plasma current, but directly measured time-resolved validation remains elusive [24]. Furthermore, the Kotsonis and Ghaemi experiment uses voltage frequencies an order of magnitude lower than real-world applications would allow, which may impact results. Their research split the flow components into *u* (in-plane) and *v* (perpendicular) directions. Although both components show certain amounts of acceleration, the majority of acceleration is in the positive *u* direction. The authors did, however, measure positive accelerations during the downward voltage stroke and slight negative accelerations during the upward stroke as shown in Figure 2.2.

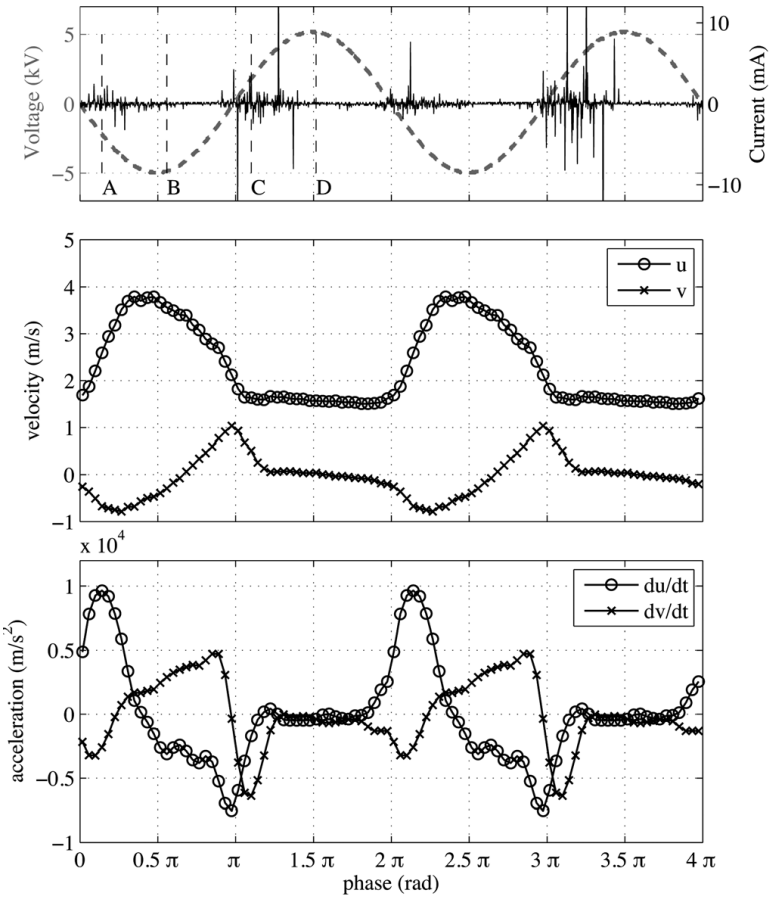

Figure 2.2. PIV time-resolved force measurements (from [24])

DBD plasma actuators create noise when actuated due to electrostatic effects. It is theorized by Mertz and Corke that the acoustic effects can be used to create a time-resolved force model of an actuator [25]. Their research consisted of setting up an array of sensitive microphones surrounding an actuator during activation and measuring the acoustic byproducts, including frequency response and phase. The results of their analysis yielded a push-pull force (see Figure 2.3), in disagreement with their previous work, indicating that more investigation into the problem is necessary.

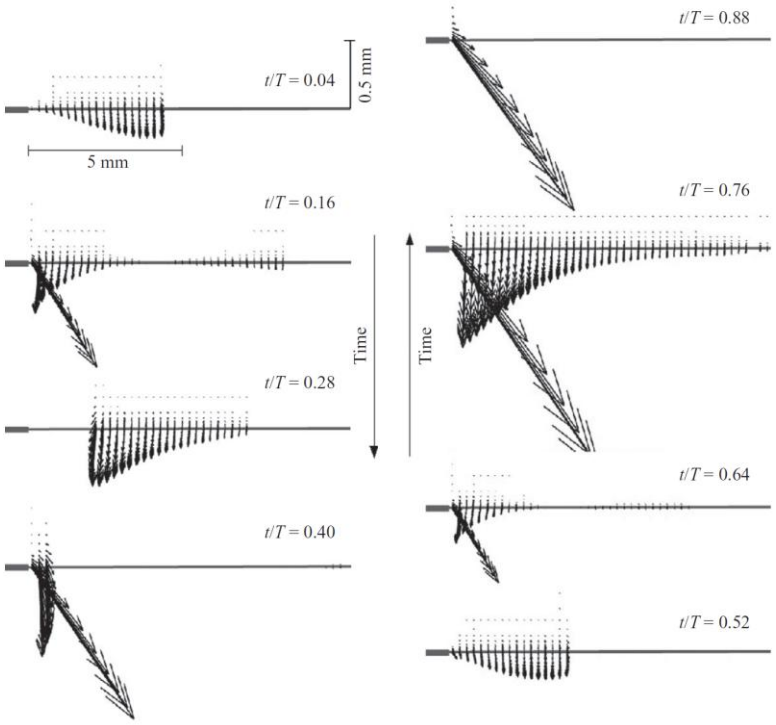

Figure 2.3. Time-resolved force model based on audio analysis (from [25])

In order to capture the time-varying force profile, a force sensor will need to have resolution of fractions of a gram and a bandwidth several times larger than the drive frequency of the DBD. There are no sensors available with that combination of resolution and bandwidth. The alternative approach developed by Font [18] is to mount the actuator so that the time-varying force accelerates the actuator to result in a time-varying position. The position can be measured remotely with sub-nanometer resolution and MHz bandwidth using laser interferometry. Based on features of the measured position signal, characteristics of time-varying force can be inferred. However, the Font method is also run at low frequencies (of a few hundred hertz), so it, too, does not agree with real-world application specifications.

3. HARMONIC RECONSTRUCTION METHODOLGY

3.1. BASIC METHODOLOGY

The approach proposed here builds on the Font [18] method with the goal of obtaining quantified, high resolution measurements of the time-varying force. Our method is to attach mechanical resonators to the actuator, with each resonator tuned to a harmonic of the time-varying force. The harmonics are determined by multiplying an integer times the base frequency. For example, if the original plasma generating frequency is at 3 kHz, then higher order harmonics include 6 kHz, 9 kHz, etc. The amplified motion of each resonator is measured by a laser interferometer. Using dynamic models of the apparatus, the time-varying force can be reconstructed from these measurements. The key benefit of this approach is the use of harmonic signals that can be averaged over many cycles to obtain very low noise. Combined with the mechanical amplification, the approach can yield very precise estimates of the time-varying force profile.

Signals, whether they take their form from force, displacement, voltage, or otherwise, can be deconstructed and separated into their component frequencies. In normal use, such a method is called frequency analysis and is simply the conversion of a time domain signal into a frequency domain signal. The utility of converting signals into the frequency domain is very high. For example, frequency domain information can clue one into any particular resonant mode, identify powers and magnitudes of signals, and also provide the means for discovering phase. Electrical circuits, audio recordings, and vibrational analysis all heavily rely on data analysis in the frequency domain.

The opposite of separating a time domain signal into the frequency domain is also true: individual frequencies with known amplitudes, frequencies, and phases, can be reconstituted into their parent time domain signal. The backward-forward manipulation of signals comes from the mathematics of the Fourier series, which explains why such a method works. Recall that any periodic signal can take the form of

$$f(t) = a_0 + \sum_{1}^{\infty} a_k \cos(k\omega t + \phi_k) \tag{3.1}$$

where a_k is the amplitude of the k^{th} harmonic of the signal, ω is the fundamental frequency, φ_k is the phase of the k^{th} harmonic, and t is time. A Fourier series represents a sum of a signal at any number of frequencies. A classic case, for example, is the reconstruction of a square wave using a sum of sine waves at particular harmonic frequencies.

Using frequency data to reconstruct a signal into the time domain at particularly selected harmonic frequencies is called harmonic reconstruction. The use of looking at harmonic frequencies in the scope of this research is to isolate frequencies of interest based on the driving voltage of the DBD actuator. For example, take the periodic function simulating nanometer displacement of a possible force on a DBD actuator represented by

$$y = 9.992^{-9}\sin(3000 * 2\pi t - 1.66958) + 6.21^{-9}\sin(6000 * 2\pi t - 1.89194) \tag{3.2}$$

which contains two signals. The plot would appear as Figure 3.1 in the time domain.

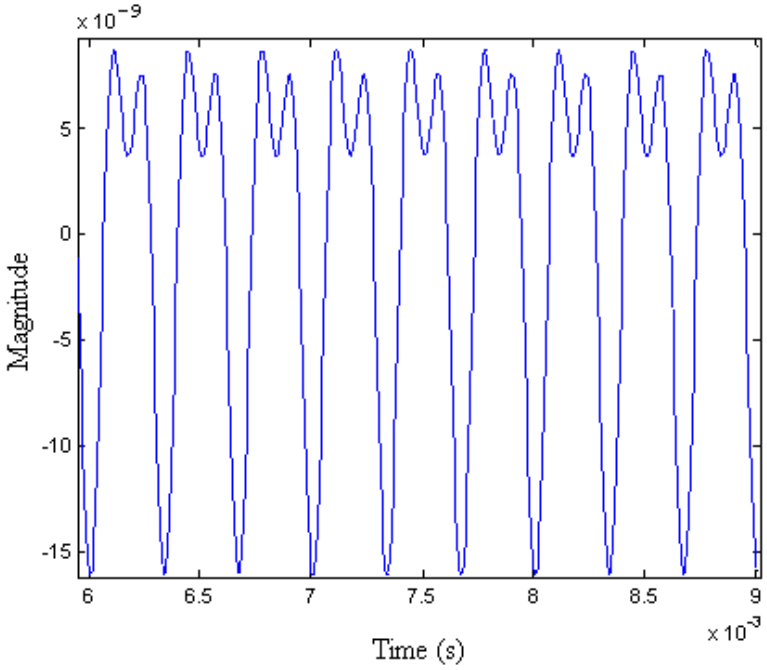

Figure 3.1. Example of a small magnitude periodic signal

When converted into frequency information via a Fourier transform, the same signal appears as Figure 3.2.

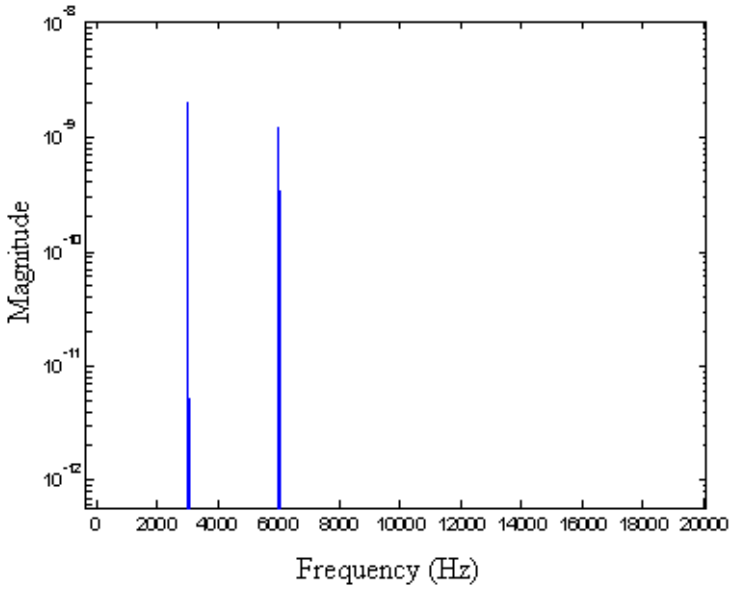

Figure 3.2. Frequency analysis of figure 2 from 0 to 20kHz

The two spikes are at 3000Hz and 6000Hz, respectively, with corresponding magnitudes.

3.2. MODELING THE PENDULUM APPARATUS

The objective of the research presented here is to determine the DBD actuator force by measuring the displacement of the actuator when it is freely hanging. To accomplish modeling of the experimental setup, the freely hanging actuator, suspended by wires, is assumed to behave like a pendulum.

The DBD plasma actuator is mounted to a rigid rectangular material, referred to here as the actuator body, as shown in Figure 3.3. The body is hung like a porch swing; that is, a support wire is attached to each corner of the body, with the pair of wires on each side forming a triangle orthogonal to the body.

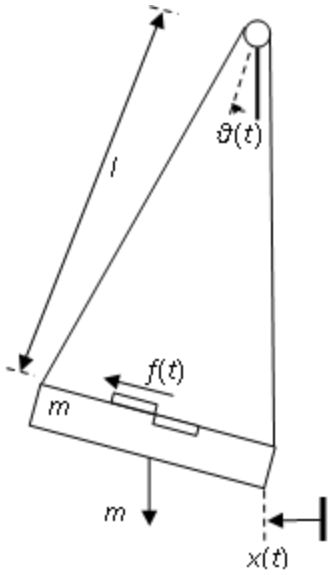

Figure 3.3. Physical setup of a freely hanging DBD actuator

In Figure 3.3, *m* is the lumped mass of the body, *l* is the distance of the body to the point of attachment, θ is the angle of rotation of the body, *x* is the horizontal displacement of the body, *f* is the thrust force provided by the DBD actuator and *g* is gravitational acceleration. Assuming that the actuator body behaves as a point-mass, the dynamics of the body are given by the pendulum equation,

$$ml\ddot{\theta} + mg\sin\theta = f \tag{3.3}$$

Drag forces are neglected because velocities are very small. Linearizing (3.3) at the DC actuator force f_0, yields,

$$ml\ddot{\hat{\theta}} + kl\hat{\theta} = \hat{f} \tag{3.4}$$

where $\hat{\theta} = \theta - \theta_0$, $\theta_0 = \sin^{-1}(f_0/mg)$, $\hat{f} = f - f_0$, and $k = (mg/l)\sin\theta_0$. For small rotations, $x \approx l\theta$ so (3.4) can be written in linear coordinates as

$$m\ddot{\hat{x}} + k\hat{x} = \hat{f} \tag{3.5}$$

where $\hat{x}$ is the differential linear motion measured from the DC offset. Taking the Fourier transform of (3.5) yields,

$$X(j\omega) = -\frac{1}{m\omega^2 - k} F(j\omega) \tag{3.6}$$

where X and F are the Fourier transform of $\hat{x}$ and $\hat{f}$, respectively. For analysis at high frequencies in the kilohertz range and above, (3.6) is approximated by,

$$X(j\omega) \approx -\frac{1}{m\omega^2} F(j\omega) \text{ or } \omega \gg \sqrt{k/m} = \sqrt{f_0/ml} \tag{3.7}$$

Equation (3.7) provides the foundation for reconstructing DBD force from body position measurements. The motion X is inversely scaled by the body mass and frequency squared. The length, l, of the wire supports are not critical as the frequencies, ω, of interest are in the range of thousands of rad/s, yielding a very good approximation in (3.7) independent of l. Maximizing motion is desired to improve the fidelity of the measurements, and so, as is intuitive, a small mass should be used.

Rigidity, or the ability of a material to withstand flexural stress, is needed to allow sufficient surface-based vibrations to pass cleanly through the body so that any mechanical resonator mounted underneath or in-plane can react with the full energy and phase of the vibration. Furthermore, highly rigid materials allow for higher bandwidth of vibrations to pass through before the material begins to move out of phase with a surface-based vibration. One example of the importance of rigidity can be found by pushing the top cover of a dictionary resting on a desktop back and forth; if the cover is pushed very slowly, the dictionary will move across the desk at the speed with which it is forced. As the speed of the forcing increases, the bottom cover of the dictionary will eventually start to lag behind the top cover. Indeed, it takes little speed to get the top cover to move

laterally while the bottom cover moves little or not at all, an indication that the rigidity of the dictionary won't pass through quick motions. Furthermore, as will be discussed, thickness also plays a role in choosing actuator body material.

Dense materials, such as metals, offer good rigidity, malleability, and low cost; however, metals have a high mass penalty and would require more energy to detect any motion. Although ceramics are often used in DBD actuator research, high cost and difficulty to machine preclude their use. Still, those materials were investigated for their horizontal shear strengths which necessarily allow for pass-through of high frequency vibrational energy.

In normal engineering textbook beam problems, beams are loaded vertically- that is, the loads point straight down into the beam, causing bending in the vertical. In the case of a horizontally mounted DBD actuator, the distributed load (plasma force) is horizontal across the top of the beam. This changes the shear direction from the horizontal to the vertical, which changes the modal vibration direction from a lateral direction to a vertical direction. As shown in Figure 3.4 and Figure 3.5, the DBD actuator body will experience shear forces due to surface plasma vibrational energy not in the x-direction, but in the y-direction.

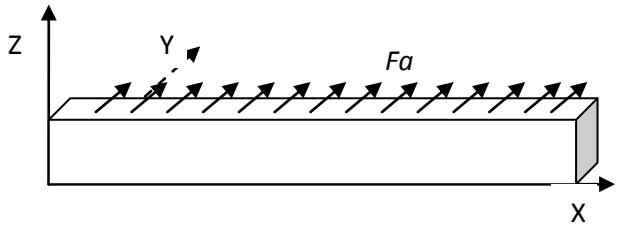

Figure 3.4. Profile view of DBD actuator body force

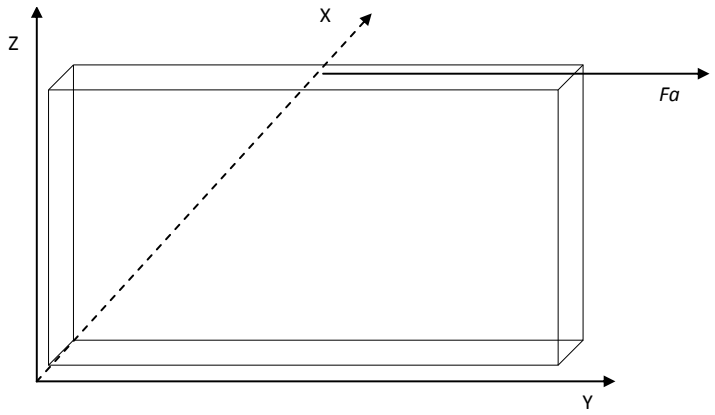

Figure 3.5. Cross-sectional view of DBD actuator body force

By applying the shear and moment forces as a function of time, the potential for vibrations and the resultant frequencies at which they pass through can be examined. In a planar DBD actuator, although the shear changes axis from x to z, it is shearing in the direction of the relative thickness of the actuator body. Consequently, the distance in the y direction can be considered as thickness and the z direction as length. Recall that the frequency equation of vibrating motion for a beam is

$$f = \frac{1}{2\pi}\sqrt{\frac{k}{m}} \tag{3.8}$$

Note that in (3.8), the frequency at which a material can transmit is inverse to its mass. For a rectangular beam, k is dependent on the physical dimensions and modulus of the structure:

$$k = \frac{E * w * thick^3}{4 * l^3} \tag{3.9}$$

As shown in (3.9), the constant k is cubically related to thickness and linearly related to

Young's modulus of the material and the width of the material. For different materials of a simulated DBD actuator body 12 in. long by 3 in. wide and 1 cm. thick, the frequency at which the actuator can transmit through itself can be calculated. Table 3.1 shows the first resonant frequency at which point the material begins to no longer pass through vibrations without a phase shift.

Table 3.1. Material properties for DBD actuator body material

Material	Calculated K	Thickness (m)	Mass (kg)	Frequency (Hz)
Magnesium	1.8828E+14	0.01	0.19703	4919892
Aluminum	2.92879E+14	0.01	0.31293	4869012
Copper	5.43919E+14	0.01	1.033828	3650589
Gold	3.26351E+14	0.01	2.23687	1922394
Iron	8.82822E+14	0.01	0.90402	4973563
Lead	6.69438E+13	0.01	1.30967	1137875
Platinum	7.0291E+14	0.01	2.48026	2679301
Mullite	5.98311E+14	0.01	0.33611	6714950
Styrofoam	4.18399E+11	0.01	0.01159	956255

Although mullite silicate yields the highest frequency pass-through, low-density Styrofoam offers the least mass penalty. Therefore, a rigid Styrofoam body appears to be a good tradeoff of mass and rigidity, particularly for the frequencies used with DBD actuator plasma, which on the order of a few kHz, are far lower than the maximum allowable frequency of the material. The primary challenge in reconstructing the DBD force from the position measurements is the scaling that can result in very small motions for high frequencies, making accurate measurement difficult. Mechanical resonators attached to the actuator body can alleviate this challenge by greatly amplifying the motion.

3.3. MODELING THE MECHANICAL RESONATORS

Simulations through MATLAB's SIMULINK software assuming a DBD actuator mass of 8.5 grams, a pendulum length of 1m, and a force of 0.25 grams operating at 3kHz yielded motions on the order of one nanometer. A nanometer, 10^{-9} meters, is a significantly small unit to detect and measure. Thus, there exists a need to amplify the vibrational displacements of a DBD actuator in order to more easily measure them. The method of choice to amplify small motions for this research is the use of small mechanical resonators. Mechanical resonators can amplify motion by excitement at a resonant frequency.

The application of mechanical resonators to amplify motion can only occur if the resonant frequency of the resonator is known. Fortunately, resonators can be manufactured to virtually any size, from large macroscopic scales to nanometer scales. Furthermore, there are a variety of architectures that can be used to create a mechanical resonator, for example, a single-clamped beam with one end fixed and one end free [26]. Unfortunately, although the single-clamped beam is perhaps the most simplified, the beam will be constantly flexing in and out of plane, making interferometry measurements (off of a reflective surface) unreliable. One critical design path for a resonator to operate in-plane is to ensure the resonance occurs in the same direction as the driving force without pivoting, rotating, or twisting. The simplest design of a resonator that keeps the resonant surface in plane is the double-clamped beam, illustrated in Figure 3.6. The boundary conditions at each end of the beam are assumed to be fully clamped so that deflection and angle of deflection are both zero.

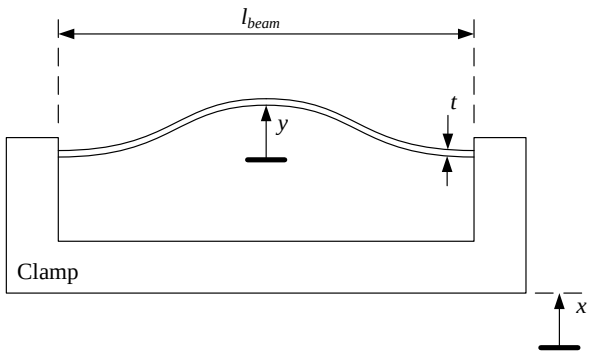

Figure 3.6. Double-clamped resonator schematic

The resonant frequency for a double-clamped beam is well known[27] and given by,

$$\omega_{beam} = C\sqrt{\frac{E}{\rho}}\frac{t}{l_{beam}^2} \tag{3.10}$$

where ω_{beam} is the resonant frequency in rad/s, C=1.03 is a beam constant, E is Young's modulus for the material selected, ρ is the density of the material, t is the thickness of the beam, and l_{beam} is the length of the beam. A calibration procedure will be used to obtain the amplification factor, Q (from equation (5.1)), and phase shift, ψ, of the resonator at its resonant frequency. These parameters allow us to find the relationship between the clamp motion, x, and amplified beam motion, y, as,

$$Y(j\omega_{beam}) = Qe^{j\psi}X(j\omega_{beam}) \tag{3.11}$$

To maximize the amplification factor, the beam thickness, t, should be kept small. The resonant frequency of the beam can be most easily adjusted by selecting the proper beam length.

3.4. FORCE RECONSTRUCTION VIA HARMONIC POSITION MEASUREMENTS

In this chapter, so far, the groundwork for combining harmonic reconstruction methodology, pendulum physics, and mechanical resonator theory has been described. Combining all three topics represents the experimental setup used to amplify, measure, and analyze small motions experienced by a plasma actuator during use. The method presented in this research contains tuned harmonic resonators designed to resonate at the driving AC voltage frequency, plus additional mechanical resonators tuned to the higher harmonics of the driving frequency. By adding the frequency content of the resonators at the driving frequency and the harmonics together, one can see a well-resolved displacement waveform. Recall from basic physics that

$$F(t) = ma(t). \tag{3.12}$$

Also,

$$\frac{dv}{dt} = a\ . \tag{3.13}$$

Since v is the time derivative of position, once a time-based position is well-resolved, the time-based acceleration is readily apparent. The mass of a DBD plasma actuator can be measured, and thus a time-varying force can be determined. Reconstruction of the time-varying force involves manipulation between the time domain and frequency domains.

Recall that actuators rely on cyclical AC voltages to operate, generating cycles of plasma at precise intervals which repeat themselves. Consequently, the body force experienced by the actuator will also follow a cyclical pattern, directly correlated with the frequency of the driving voltage, given by ω_0. It then follows that the time-varying force can be written as a sum of harmonics in the time domain as

$$\hat{f}(t) = \sum_{k=1}^{\infty} c_k \cos(k\omega_0 t + \phi_k), \tag{3.14}$$

or, in the frequency domain,

$$F(j\omega) = \sum_{k=1}^{\infty} c_k \delta(k\omega_0) e^{j\phi_k} \tag{3.15}$$

where δ is the impulse function, $\delta(\omega) = 0$ for $\omega \neq 0$, and $\int_{-\infty}^{\infty} \delta(\omega) d\omega = 1$ for any ω>0. From (3.7), (3.9), and (3.15), the motion of a resonator tuned to resonate at the k^{th} harmonic frequency is given by,

$$\begin{aligned} Y(jk\omega_0) &= -\frac{c_k Q_k}{mk^2\omega_0^2} e^{j(\psi_k + \phi_k)} \delta(k\omega_0) \\ &= \frac{c_k Q_k}{mk^2\omega_0^2} e^{j(\psi_k + \phi_k + \pi)} \delta(k\omega_0), \end{aligned} \tag{3.16}$$

and therefore, magnitude and phase measurements of the k^{th} harmonic resonator are given by,

$$Mag(k) = \frac{c_k Q_k}{mk^2\omega_0^2}, \tag{3.17}$$

and,

$$Phase(k) = \psi_k + \phi_k + \pi. \tag{3.18}$$

The time-varying force coefficients can then be calculated as,

$$c_k = \frac{mk^2\omega_0^2 Mag(k)}{Q_k}, \tag{3.19}$$

and

$$\phi_k = Phase(k) - \psi_k - \pi \tag{3.20}$$

In order to determine the accuracy of the reconstructed force, let R be the resolution with which the magnitude of the resonator motion can be measured. Then, the

differential error in the k^{th} harmonic of the force is given by,

$$c_k = \frac{mk^2\omega_0^2 R}{Q_k} \tag{3.21}$$

Clearly, large resonator amplification gains (Q_k) will be necessary at high frequencies (ω_0) to accurately reconstruct the force.

An important practical question to answer is how many harmonics are needed to accurately recreate the force waveform. This, of course, is difficult to determine without a precise model of the time-varying force. However, previous works [6,7] have determined that PUSH-push profiles, containing one large push and one small push in each cycle, are common. A candidate PUSH-push force profile was constructed, and is illustrated in Figure 3.7. The fundamental frequency for this candidate is 3000 Hz. The Fourier magnitude and phase coefficients are shown in Figure 3.8 and Figure 3.9 which shows that the response is dominated by the first three harmonics.

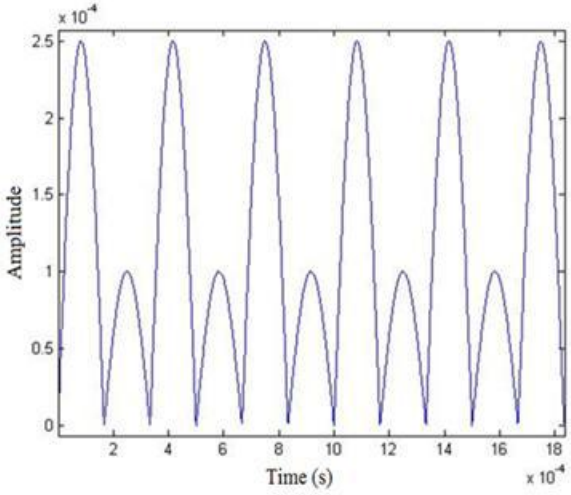

Figure 3.7. Candidate PUSH-push force signal

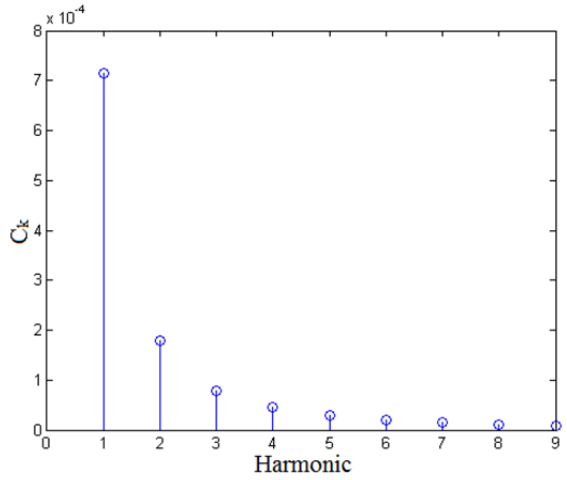

Figure 3.8. Coefficient vs. harmonic number

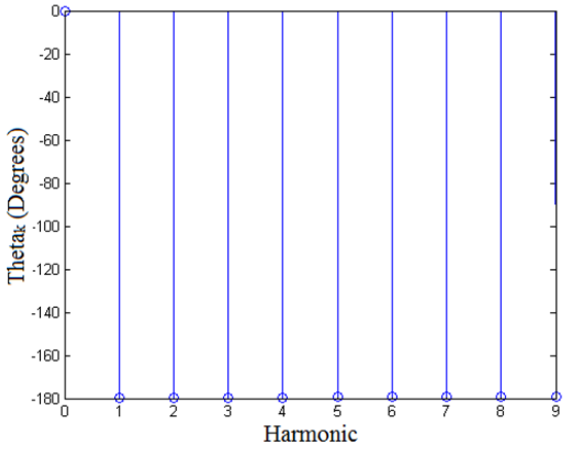

Figure 3.9. Phase vs. harmonic number

A reconstructed force profile containing only the first three harmonics is shown in Figure 3.10, which demonstrates good agreement with the original signal. Note that although the sharpness of the peaks are slightly more rounded, the magnitudes are in good agreement in the reconstructed signal, indicating a good fit. Thus, as little as three mechanical resonators are required in order to accurately reconstruct a candidate PUSH-push force profile.

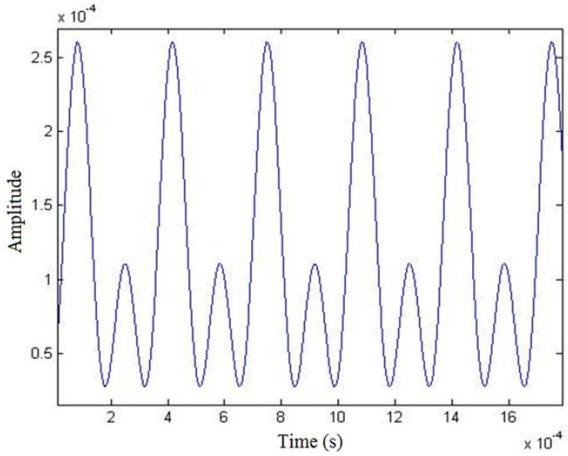

Figure 3.10. Reconstructed PUSH-push force signal (3 harmonics)

4. EXPERIMENTAL SETUP

4.1. LASER INTERFEROMETRY

The experiment performed in this research requires instrumentation that, first and foremost, can detect sub-nanometer displacements. Instrumentation that can capture a high bandwidth of information is also necessary. High bandwidth sensing is required in order to fully resolve displacements that occur within each plasma oscillation. For example, if the driving AC voltage is at 3000Hz, a sampling rate of 30000Hz would yield ten datapoints of displacement per cycle. Also, instrumentation that does not need to be physically connected to the source (here, the DBD actuator) is desirable. Instrumentation that requires direct connection to the actuator would serve as additional mass, potentially several times greater than that of the actuator itself, and would only dampen any vibration that the actuator is experiencing.

Within several manners of nanoscale displacement detection, two of the most commonly used involve reflected light (such as from a laser) and inductance from capacitors. In terms of reflected light, interferometers use the phase difference between a reference beam and a reflected beam in order to determine displacement. Another version uses interdigitated diffraction gratings- two gratings which allow light to pass through a static “comb” while reflecting off of a dynamic interwoven “comb”, forming a diffraction pattern. A photodiode uses the reflected pattern to determine displacement, frequently used in atomic force microscopy [28]. Capacitance displacement sensors measure inductance in two plates to determine displacement to a remarkable resolution- insofar as mass and resonance of the system does not matter. Both methods have inherent strengths and weaknesses which are detailed in Table 4.1.

Table 4.1 Sensors investigated and their specifications

	Max Resolution (nm)	Sensor Distance to Target	Spot Target Size	Bandwidth
Laser Interferometer[29]	.072	1mm-1m	3 microns (at 1mm) 3-5mm (at 1 m)	6.5 MHz
Interdigitated Cantilevers[30]	.001	2.2mm	20 microns	1 kHz
Capacitance Sensor[31]	.01	150 microns	2.3mm	10 kHz

In summary, the interdigitated cantilevers provided the best resolution but the worst bandwidth. Capacitance sensors have excellent resolution at an acceptable bandwidth, but add mass to the system along with an extra tether, rendering its use invalid for our setup. The final instrument to consider is laser interferometery, which has a very high bandwidth and is fully non-contact, but does not have as good of resolution compared to the others.

Due to excessive mass addition, the capacitance sensor must be disregarded. Alternatively, the interdigitated cantilever system must be discounted as well due to insufficient bandwidth. The laser interferometer, then, becomes our best choice for our experiment. However, standard laser interferometers lack the resolution needed for our application (generally speaking, resolution of an unaided interferometer is on the order of 1-10 nm), and to compensate, a high-resolution analog interpolation device shall be used. Figure 4.1 is a schematic of the experiment with electrical equipment and optics setup.

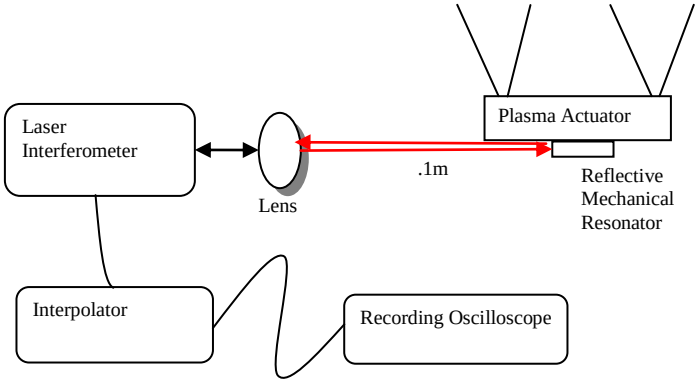

Figure 4.1.Interferometer equipment setup

Laser interferometry involves taking a laser beam of precisely known wavelength (most often a helium-neon laser with 633 nanometer wavelength), and splitting the beam to reflect off of an internal retroreflector and an external measurement surface. The externally reflected beam is allowed to recombine with the internally reflected beam inside the interferometer, and phase changes produce either constructive or destructive interference. The interference patterns of the recombined laser beam allow the interferometer to determine the direction of travel, either towards or away, and the amount of travel inherent to the native resolution of the interferometer. Interferometer systems, as noted above, have excellent resolution and bandwidth, and are fully non-contact in a plane-mirror configuration.

Several vendors of interferometry equipment are widely used in industry, but for this experiment Renishaw is selected because of cost, performance, and compatibility with existing equipment. Sensing of the resonator displacement is accomplished with a Renishaw model RLE10-SX-XD plane mirror laser interferometer, coupled with a Renishaw REE4000A50A quadrature interpolator. The minimum resolution output of

the RLE10-SX-XD unit by itself is 20 nm. Based on a helium-neon laser with a wavelength of 633 nm, the REE4000A50A interpolates the interferometer output down to a final resolution of exactly 0.0791 nm.

Laser interferometers from the vendor selected for this research comes in two different configurations. One configuration uses a retroreflector which can be mounted to a surface. The retroreflector uses internal optics that allow for a direct reflection, in plane, to return the laser beam back to the source. No other optics are necessary with this configuration; however, the retroreflector has mass that would have to be added to the detected surface. The other configuration is a plane mirror interface. In the plane mirror configuration, an external collimating lens is required to focus the outward laser beam to a minimum radius (the laser beam itself is 3mm wide), and thus also dictates the reflective target must be of certain distance from the lens, unlike in the retroreflector configuration. Also, in the plane mirror configuration, a reflective surface with a roughness of 20 nanometers or less is required. For this experiment, due to mass restrictions, the retroreflector configuration is not an option; instead, the plane mirror configuration is selected. Clearly, that selection will dictate a restricted selection of resonator material: machinable metal chosen must have a mirror-smooth surface. Fortunately, polished stainless steel has desirable properties that make it well suited for this experimental application.

The Renishaw interpolator unit has an output rate of 50MHz, requiring a digital oscilloscope capable of recording at least 100MHz (the nyquist frequency). A Tektronix DPO2024 4-channel recording digital oscilloscope is used to store up to 10ms worth of

interferometer output, with a memory large enough to store 1.25 million data points, at a minimum sampling rate of 125MHz.

In order for the interferometer to receive an adequate signal from the mechanical resonator, a reflectivity value of at least 50% is needed. Highly polished stainless steel is ideal for this application: the interferometer routinely detects 60% reflectivity or better. The digital quadrature output from the interpolator takes the form of a +/-5V square wave, requiring a post-processing program to decode the voltage into discrete steps. Displacement measurement is then derived from the status of the steps by comparing which channel (A or B) transitions before the other. MATLAB code is used extensively for this purpose, with an added benefit of precisely plotting voltage waveform input and plasma current on the same plot as displacement. Data processing and interpretation will be discussed in greater detail later in this chapter.

4.2. RESONATOR DESIGN

Several types of resonators were examined for use in this research. Initially, a micron-scale silicon-on-oxide custom fabricated resonator was examined. Such a resonator would have taken the shape of a single-clamped beam hanging from its top in a frame. All surfaces would have had the capability of being manufactured in a focused ion beam fabricator which would have removed any non-reflective surface, leaving behind a mirror-smooth silicon surface. The dimensions would have been precisely calculated, and then created on a silicon wafer, much like how White[32] created micron-scale silicon thermal actuators. The benefits of such a construction would have been precise control over the manufacturing process, a small, low-mass resonator, and a highly

polished reflective surface. The drawbacks included time to manufacture, the fragile quality of silicon, and the high cost to fabricate. A double-clamped, lumped center mass cantilever design was also examined, as shown in Figure 4.2.

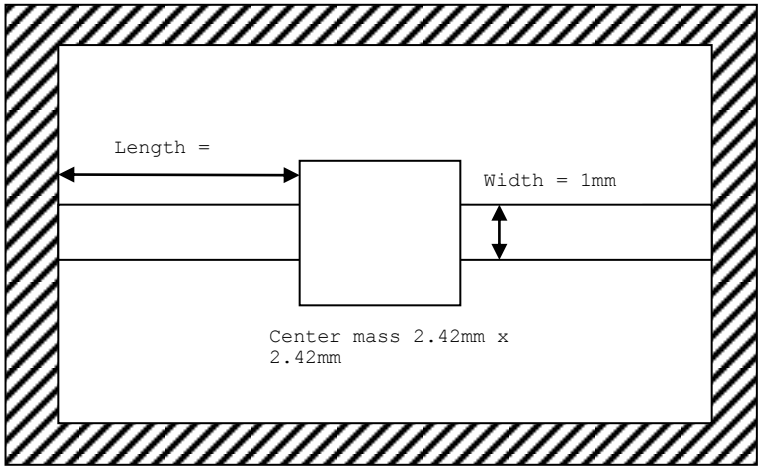

Figure 4.2. Center-mass double-clamped cantilever candidate design

Taking a double-clamped, lumped center mass micron-scale resonator and scaling it to millimeter or centimeter size seemed feasible. The benefits of such a design included a target size large enough to work with an interferometer system easily, and greater tolerance to adjust the resonator frequency by adding or subtracting mass from the center. Initially, a fully silicon-on-oxide ion beam fabrication was considered. However, like all silicon fabrications, manufacturing standards are exact and quite high. Although silicon, with a high resonance amplification (or Q) factor would have been an excellent mass-to-performance tradeoff, stainless steel, with its low cost and easy machinability, was selected.

Stainless steel is widely available in a vast variety of shapes, thicknesses, and finishes. For this application, the thinnest stainless steel available in a mirror polish is

used, a thickness of .03", procured from McMaster-Carr. From equation (3.10), it is clear that the resonant frequency of a double-clamped beam varies inversely square with length and directly with thickness. Stainless steel with a mirrored finish at a thickness of .03" is the thinnest commercially available, allowing for the largest possible area of resonator and ease of fabrication, installation, and use with an interferometer system. Figure 4.3 shows the first iteration of a double-clamped beam using mirrored stainless steel as a medium.

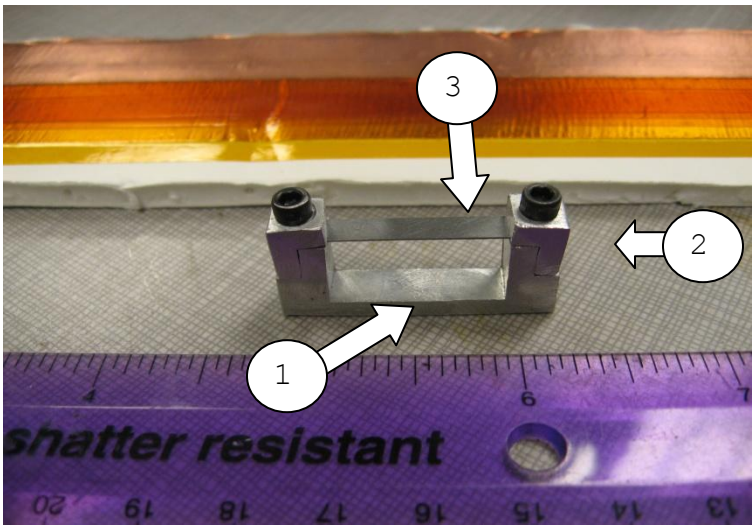

Figure 4.3. Original resonator and clamp assembly

The clamp base is machined aluminum (1), and the L-shaped clamps are secured with standard hex screws (2). The stainless steel resonator itself (3) is securely clamped down. L-shaped clamps were chosen to prevent the clamps from torquing when screwed into place, thus maintaining as rigid and full of a clamp on the resonator beam as possible. This design had one significant flaw: small gaps were formed between the clamp base and clamps themselves when screwed into place. The gaps allowed for the

clamps to pivot outward, away from the beam. As a result, the boundary conditions for the resonator were impacted. Instead of maintaining constant resonator length, the resonator experienced motion beyond the inside edge of the clamps, impacting the resonant frequency due to the sensitivity of the length parameter. Repeatability of a resonant frequency was low; removing the clamps and reinstalling them impacted the frequency response.

Other methods of securing the ends of the resonator were investigated. The ideal solution maintains a constant resonator length, eliminating the outward pivoting of the L-shaped clamp ends. Thus, methods to prevent the clamps from pivoting are necessary. Instead of using L-shaped clamps, a clamping mechanism impervious to torquing or pivoting was developed that ensures integrity of the resonator length by eliminating the ability of the clamps to rotate or pivot. Figure 4.4 shows the final manufactured clamp and beam assembly with a ruler for scale.

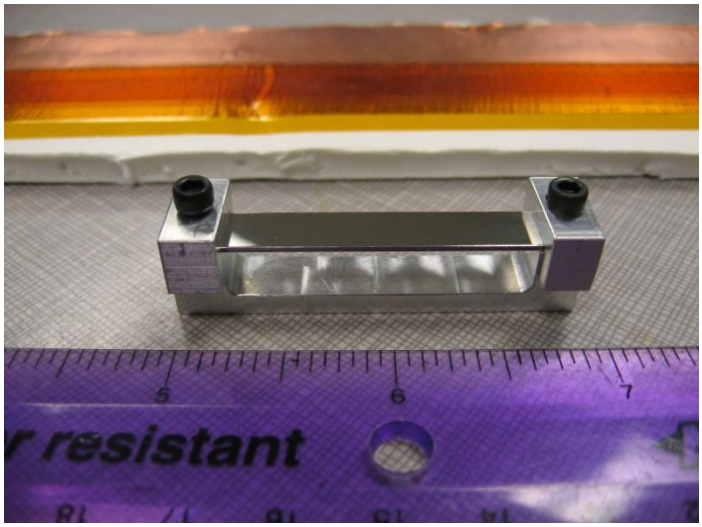

Figure 4.4. Final resonator and clamp assembly

First, the resonator beam and base was fabricated on a CNC machine to precisely cut the stainless steel. The resonator beam, instead of being one rectangular shape, had through holes cut at the ends to allow for the screws to be set through the beam. Finally, the L-shaped clamps were discarded in favor of an upside down U, precisely fitted to the base, which made torquing of the clamps impossible. The resonator design, now, allows for no excessive flexibility at the ends of the beam, maintaining control over the effective length and precision of the resonant frequency, despite repeatedly removing the clamps and reinstalling them which may impact the resonator's characteristics.

Testing of the resonator/clamp setup, at first, consisted of removing the cone from a loudspeaker and affixing the clamp base into the magnetic voice coil. A frequency sweep was conducted, running voltage to drive the speaker coil varying from 1kHz to 5kHz. A lab laser was held in place to reflect onto a nearby wall, and changes in reflected laser positioning was noted. Also, audible response was monitored to identify any frequency where the tonal qualities emanating from the resonator occurred. After a design resonance was calculated to be 2997Hz, the speaker frequency sweep revealed a resonance at 2720Hz. Also, audio recordings confirmed a range of resonance from 2645-2800Hz.

Audible testing of the resonant frequency, although successfully identifying one characteristic of the resonator, did not precisely allow for measurement of displacement or phase. In order to measure the physical displacement and phase, a more detailed method is needed. A vibrating surface analogous to the motion of a DBD actuator is needed to mount the resonator assembly. Frequency control and nanometer-scale vibrations are also desirable. Piezoeletric devices were investigated but discounted due

to high cost. Linear motors were proper in price but insufficient in frequency response. The third device, a solenoid, has the combination of price and performance that makes it suitable for this experiment.

Initially, a 45-watt solenoid-based vibration test is constructed. The solenoid is of a pull-pull variety, meaning that for each AC waveform passing through varying from positive to negative along zero volts, the solenoid will pull in with each transition as shown in Figure 4.5. So, a voltage at 3000Hz would result in 6000 pull cycles per second. The solenoid, then, must be connected to a negative DC "float" voltage that causes the driving AC feed to be fully negative during each waveform, allowing for the solenoid piston to follow the AC feed precisely. An electrical schematic of the DC "float" electronics appears in Figure 4.6.

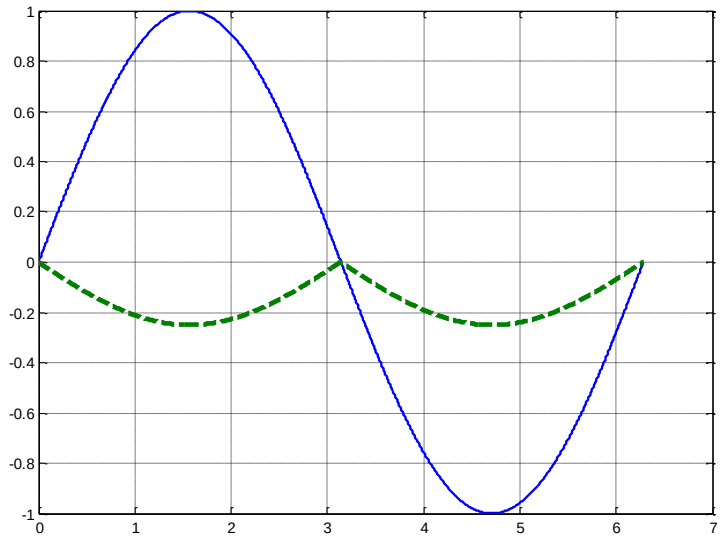

Figure 4.5. Simulated voltage (solid line) and solenoid motion (dashed) before applying DC bias

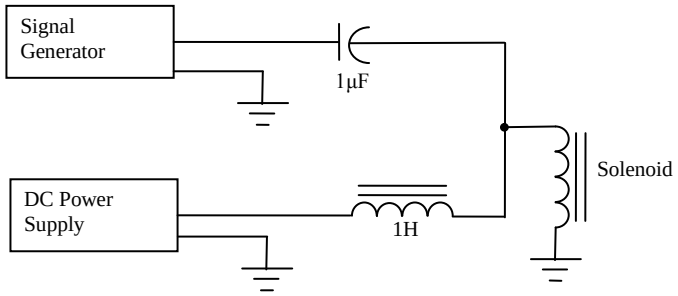

Figure 4.6. Electrical schematic of the solenoid testbed

Another issue is that the solenoid has no restoring force. So, the resonator is positioned and affixed as show in figure x and rested on a spring. The spring experiences compression with each pull cycle and acts as a restoring force, allowing the resonator to return to a zero position. The final calibration resonator setup appears in Figure 4.7.

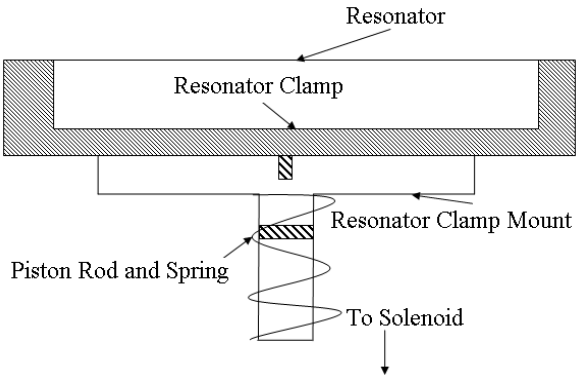

Figure 4.7. Resonator calibration setup

The resonator was used in conjunction with the laser interferometer system in order to properly measure the frequency response as determined by voltage sweeps to the solenoid. The interferometer was set to its highest resolution in order to determine the displacement and phase at different voltages at different frequencies. Full resonator

response measurements, including both frequency and phase, are presented in the next chapter.

4.3. DBD SETUP

The DBD plasma actuator is constructed of ¼" thick paper bounded Styrofoam, copper tape for the ground and positive electrodes, and three layers of Kapton tape for dielectric. Fewer layers of Kapton tape was used in early trials, but the addition of dielectric, despite adding small amounts of mass to the DBD actuator, allowed for both longer actuator lifespan and higher power levels. The dimensions of the DBD actuator are 3" wide by 10" across.

The actuator is mounted to a bolted frame apparatus which is, in turn, bolted to a large vibration isolation table. The vibration isolation table, in addition to acting as a very large filter due to its large mass, also has mechanical and oil dampers which help to further reduce extraneous vibrations. A special frame had to be constructed and installed for support of the actuator, which appears in Figure 4.8.

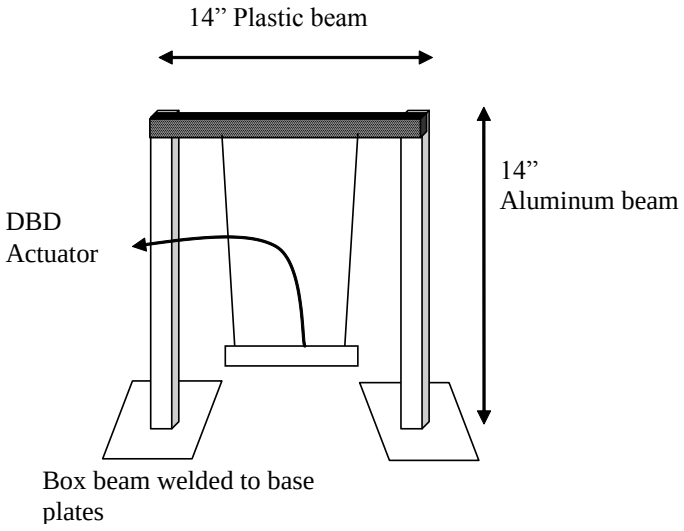

Figure 4.8. DBD actuator and stand setup

The actuator is suspended via 32 gauge enameled high voltage wire capable of 10kV at low current while maintaining excellent flexibility. The wire is attached to an insulated crossbar rod to prevent any arcing during high voltage operation. The wires are soldered to the positive and ground electrode, respectively. A reflective beam was glued to the leading edge of the actuator to maintain a profile low enough so as to not disturb any airflow across the surface of the actuator. The mass of the actuator, reflective beam, electrical components, base, and wires is 20.18 grams.

Equipment used to generate the driving voltage include a Crown CE2000 amplifier with a Rigol DG 1022 digital function generator generating voltages up to 10V AC at frequencies up to 9kHz. The output from the amplifier is sent through a fuse-protected high voltage transformer with a 200:1 step-up. A Tektronix high voltage probe model P6015, with a 1000:1 input to output ratio, is used along with a Pearson current monitor, model 4100, with a 1:1 volt to current ratio, to measure the applied voltage and plasma current from the actuator. A Tektronix DPO2024 4-channel recording digital

oscilloscope is used to record the data from those two instruments, with a memory large enough to store 1.25 million data points, or 10ms of time at 125MHz sampling rate. The digital oscilloscope is the same model used to record the quadrature output from the laser interferometer. The two oscilloscopes are set to trigger simultaneously from a triggering signal sent from the function generator when activated. Figure 4.9 is a photograph of the final experimental setup, with the DBD actuator suspended in the foreground and the laser interferometer in the background.

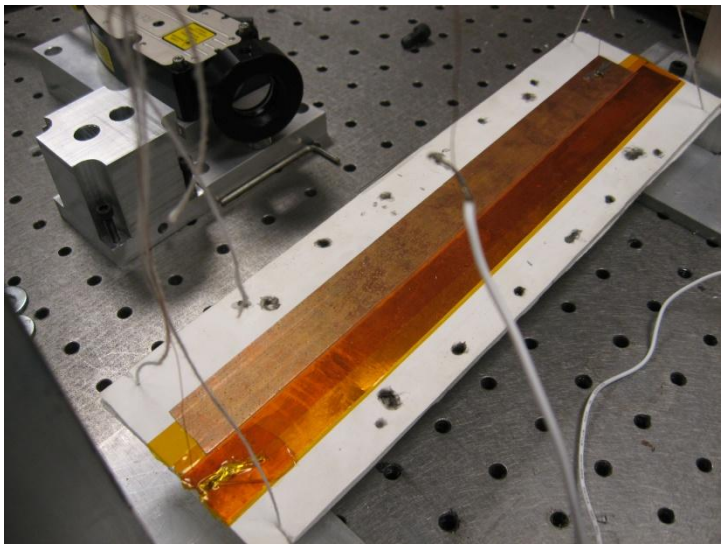

Figure 4.9. Freely hanging DBD actuator and laser interferometer

4.4. DATA PROCESSING AND INTERPRETATION

The laser interferometer is the key instrument in this experiment since it is the sensor which, ultimately, detects sub-nanometer vibration at a high refresh rate. The interferometer, however, does not explicitly output displacement; instead, it outputs a voltage signal. Recall that the interferometer reads the phase change between a reflected

laser beam and a reference beam. Nowhere along the circuitry of the interferometer is displacement actually deduced: it is up to the end user to figure out a solution to decode the electric signals output from the interferometer/interpolator setup.

The interferometer uses a series of sine and cosine voltage waves to output the relative phase changes of the incident and reflected laser beams. From these sine and cosine waves, the interpolator converts the analog signals into digital square waveforms, at the same time interpolating the resolution by a factor of 4,091 times. Whereas the minimum resolution output from the interferometer is 10 nanometers, the final output resolution of the interpolator yields a defined output of .0791 nanometers.

Displacement is based on a series of digital square waves called quadrature, or A quad B. The square waves have a peak-to-peak voltage of 5 volts and can transition at the frequency set by the interpolator of 50MHz. An example appears in Figure 4.10 below.

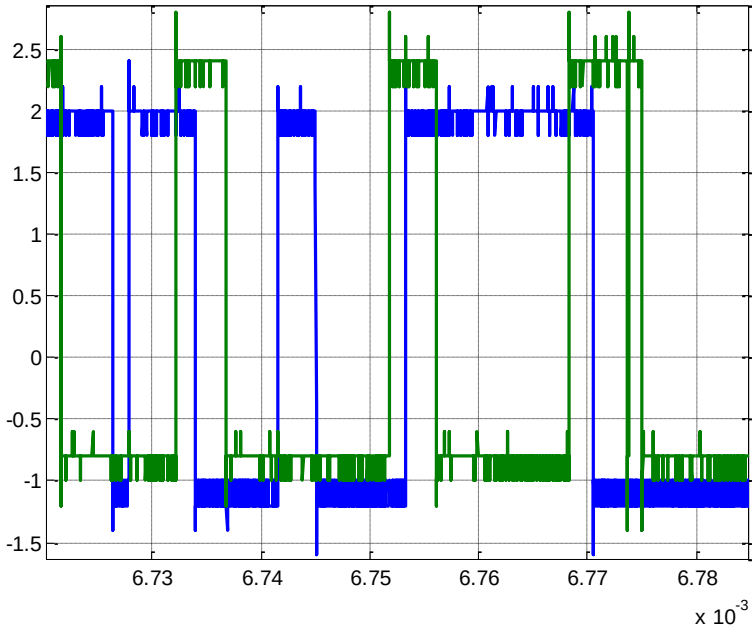

Figure 4.10. A and B channel interferometer raw voltage output

Taking the output square wave voltage and converting to displacement is a matter of programming. First, the program must decode the raw square wave voltage output and digitize the voltage into a series of zeros and ones. Since the output rate of the interpolator is set at 50MHz, the decoding program is written to look for voltage switching at speeds less than the known rate. Including a portion of code that prevents the decoding program from mistakenly identifying false voltage switching, hysteretic logic is used. This is done to prevent the program from falsely interpreting slightest instances of noise, which allows for error-free decoding even in circumstances of electrical noise. Figure 4.11 shows the digitized square wave.

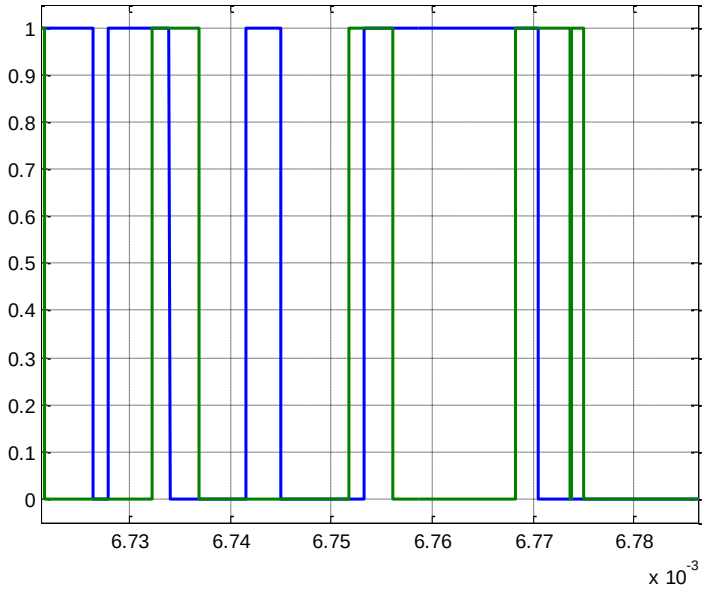

Figure 4.11. A and B channel digitized output

Next, the program looks for times that the square waves, identified as A and B, transition from zero to 1 and back again. This is the critical step in the decoding process: if A transitions positive before B without reverting back to zero, then that is counted as one step of resolution toward the interferometer. If B transitions positive before A without reverting back to zero, then that is counted as one step of resolution away from the interferometer. The same logic applies for transitions of positive to zero. The program keeps a record of times that these displacement steps occur, allowing for a position versus time plot. Error prevention is key in this step: if both channels flip at the same time or in an illogical order, the data is considered suspect, and a message flagging the user to suspect data points is printed. Even one suspect data point out of 1.25 million is cause to consider the entire dataset erroneous. In this instance, the necessity of collecting new data is indicated.

In order to calibrate the interferometer along with the computer code, the interferometer laser was mounted to a 3-axis positioning table which provided micron-scale positioning sensitivity. A stationary plane mirror target was aligned so that the reflectivity value was maximized. The digital recording oscilloscope was set to record 1 million datapoints over a span of one second. It should be noted that the interpolator was removed for this calibration because the oscilloscope could not record one second worth of data at the high output rate of the interpolator, so a slower output rate was selected directly from the interferometer unit itself. After the recording was triggered, the positioning table was manually adjusted to move 90 microns toward the plane mirror target. Figure 4.12 shows that the result of the calibration was successful: the oscilloscope correctly recorded the data, the program correctly decoded the data, and MATLAB correctly plotted the displacement versus time.

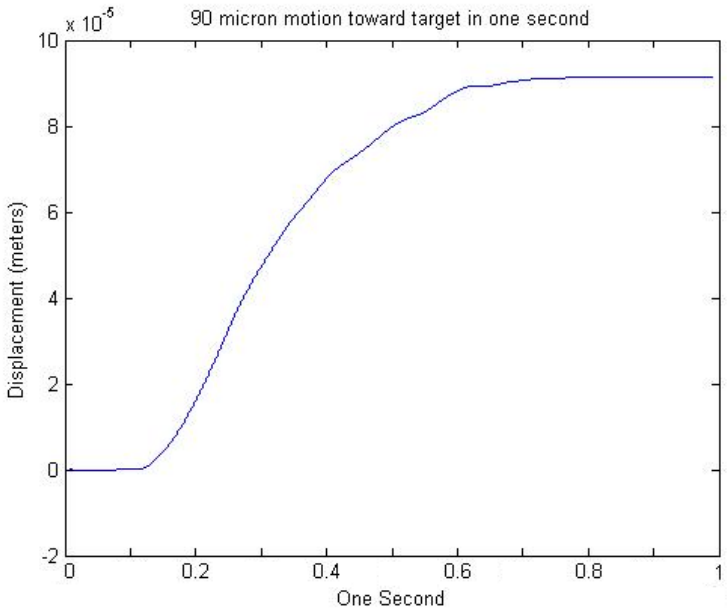

Figure 4.12. Interferometer displacement and code calibration test

Full text of the decoding program appears in the appendix. In addition to plotting displacement versus time, the position data can be filtered discretely to create a velocity plot, or can be converted to the frequency domain via a Fourier transform. Analysis of actuator vibration data appears in the next chapter.

5. RESULTS AND ANALYSIS

5.1. RESONATOR RESPONSE MEASUREMENTS

The resonator-solenoid assembly is driven by a 10V peak-to-peak sine wave, offset by 360mA to ensure true push-pull motion. Displacement is derived from measurements from a custom MATLAB interferometer decoding program, and phase is calculated by MATLAB's Fast Fourier Transform (FFT) subroutine. Trials are run from 2kHz to 2.4kHz and 2.7kHz to 3.1kHz at 100Hz intervals, whereas the intervals were reduced to as little as 1Hz between 2.4kHz and 2.7kHz to better resolve the exact resonant frequency and amplification factor. The interferometer is positioned to measure as close to the base as possible to prevent measurement of the amplified resonator motion, then moved to measure the center of the resonator, where maximum displacement is expected, without changing any other parameters. Figure 5.1 is labeled to show the base displacement measured at location 1 and the full resonator displacement measured at location 2.

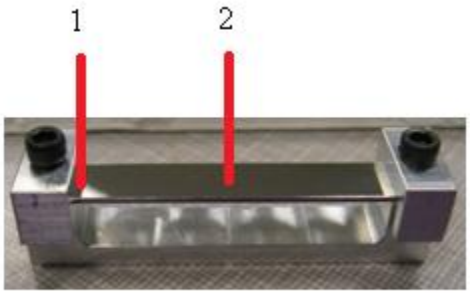

Figure 5.1. Location of displacement measurements on resonator

It is necessary to know base motion in order to compute the amplification factor at any given frequency given by the equation

$$\frac{Mag_{Beam}}{Mag_{Clamp}} = Q \tag{5.1}$$

just as phase can be calculated by

$$(\phi_{beam} - \phi_{volt}) - (\phi_{clamp} - \phi_{volt}) = \theta_{beam} \tag{5.2}$$

Beam and clamp magnitudes are determined by MATLAB FFT calculations. Figure 5.2 and Figure 5.3 shows the magnitude of resonator displacement and the phase of the resonator at frequencies from 2kHz to 3.1kHz. Ultimately, beam phase- a key parameter in determining resonant frequency- is dependent on the phase relationship between the driving voltage and difference with the phase of the clamp base. Beam phase needs to be calculated here because the beam and clamp phases could not be recorded simultaneously on account of having one interferometer.

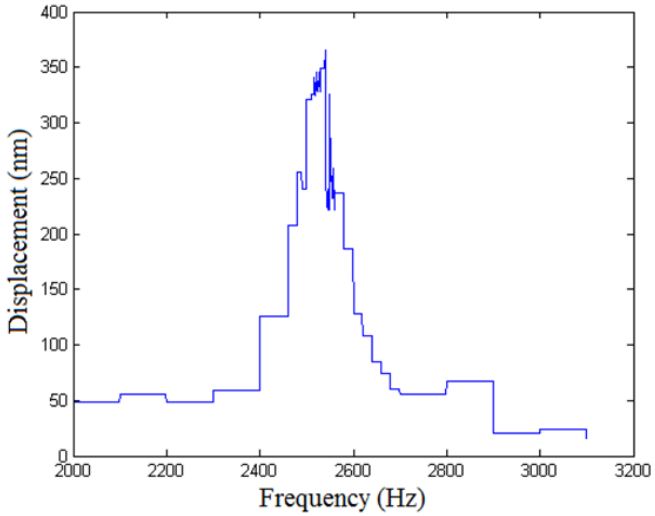

Figure 5.2. Displacement of resonator from 2000-3100Hz

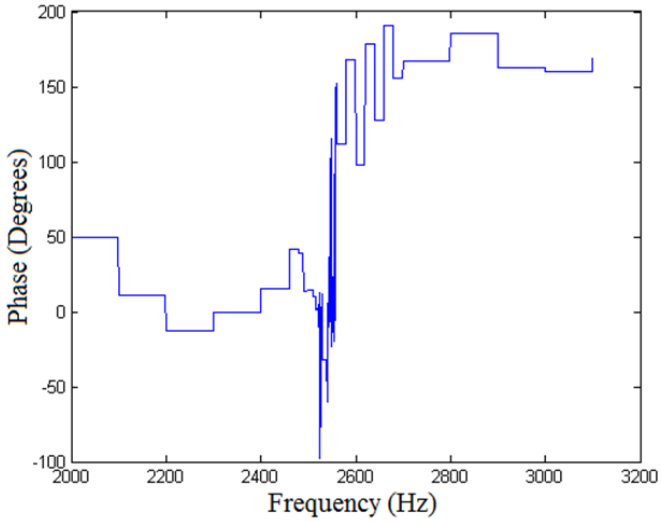

Figure 5.3. Phase of resonator from 2000-3100Hz

The data collected reflects a beam at resonance: displacement that soars at a particular frequency, here 2560Hz, along with a phase change from zero to 180 degrees at the same frequency. The measured displacements are very small, in fact, the base clamp motion is on the order of a nanometer through much of the frequency sweep. The main factor, then, is the displacement of the resonator at its center, where displacements are maximized. Figure 5.4 plots the calculated displacement amplification.

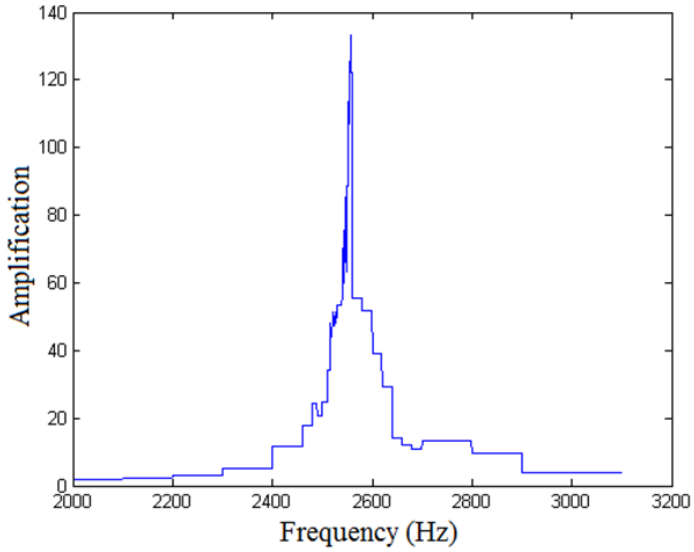

Figure 5.4. Amplification of resonator from 2000-3100Hz

The amplification factor is maximized to a factor of Q=130 times at 2560Hz, re-confirming the resonant frequency of this particular resonator. Taken into account with the maximum sensitivity of the interferometer system (0.0791nm), the amplification factor can take a base displacement as low as 6.1^{-13} meters and yield a measurable displacement at the center of the resonator. Such a displacement would be at the limit of detectable resolution, however, and base motion of a greater value is needed to fully resolve motion. Figure 5.5 shows that the base displacement can approach very small amounts in this particular setup.

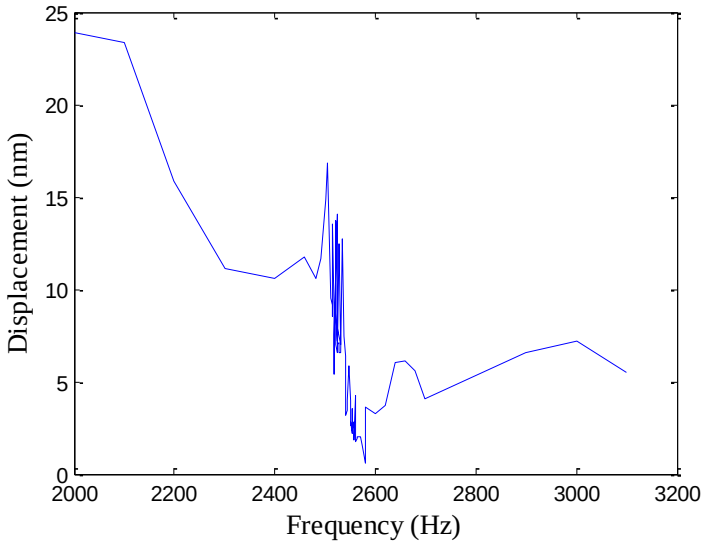

Figure 5.5. Clamp base motion

Smaller resonators designed to resonate at higher frequencies can be tested in the same manner as described above. Caution must be taken, however, when measuring displacements at higher frequencies as the clamp motion trends toward the resolution that the interferometer can measure, increasing error and potentially preventing measurement and calculation of the amplification factor. As shown in Figure 5.5, the clamp base motion trends towards 5 nanometers by 3100Hz, occasionally falling below 2 nanometers. The clamp base displacement will only continue lower as frequencies increase.

The resonator presented here can also be used to amplify any in-plane vibration up to the maximum velocity detectable by the interferometer. Piezoelectric surfaces and linear actuators, for example, are two possible applications that this resonator may be capable of amplifying, insofar as the frequency of the structure is known and can be set at the resonant frequency. Such applications would provide greater accuracy and control compared to a spring-loaded solenoid.

5.2. DISPLACEMENT MEASUREMENTS AND FORCE RECONSTRUCTION

Force reconstruction requires that the displacement of a DBD actuator be known. This experiment uses mechanical resonators to physically amplify motion. In Section 5.1, it is shown that resonators can be manufactured to amplify sub-nanometer displacements, and then recorded by an interferometer to calculate motion. There are instances where motion is large enough to be measured directly. A laser interferometer system such as the one used in this experiment has the capability of directly measuring sub-nanometer displacements of a properly set up DBD actuator without the need for attaching resonators. One must keep in mind, however, that as measurements approach the resolution of the detector, error is increased. It is shown earlier that modeling the DBD actuator yielded motion on the order of one nanometer, so although direct measurement is possible, applying resonators can improve the precision of detection and lower the potential error.

The experiment undertaken here directly measures displacement from a freely hanging DBD actuator as described in Chapter 4. The actuator is activated with 6kV, 8.5kV, and 9.3kV of AC voltage in a sine wave pattern. Recorded data from the interferometer and voltage/current instruments are analyzed in MATLAB.

Figure 5.6 shows a displacement signal as detected by the interferometer and how that same signal looks when reconstructed with FFT from 3kHz to 18kHz. The original signal experiences different offsets, which the FFT calculation removes. Also, the FFT calculation eliminates high frequency noise from the signal, smoothing it out while retaining the overall shape and curvature of the original signal. Noticeably, the FFT

reconstruction is in good agreement from run-to-run, showing that repeatability with recording DBD motion is high.

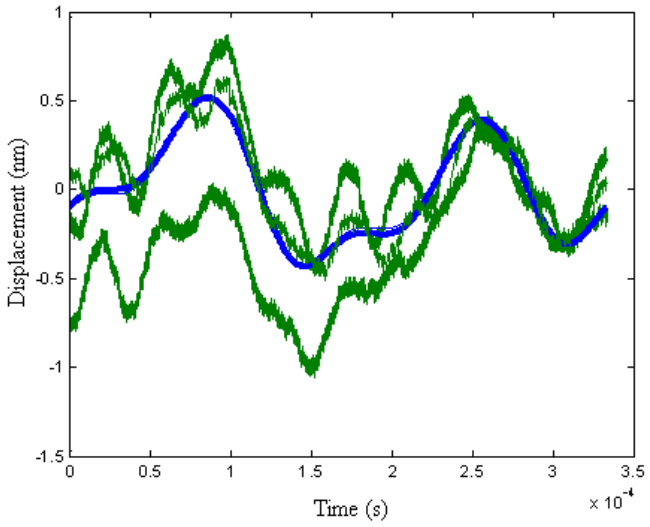

Figure 5.6. Position data from 3 runs (green) and reconstructed FFT position (blue), 9.3kV case

Position data can be time-correlated to that of driving voltage and plasma current for further examination, and plotted along with derived DBD actuator velocity. The results are shown in Figure 5.7 and Figure 5.8. In Figure 5.7, as the voltage is experiencing a maximum or minimum slope, plasma current is created, and is extinguished as the voltage reaches a maximum or minimum peak. This result is in agreement with previously performed research [2-6]. The position data, here shown processed by FFT calculation, indicates positive displacement with each plasma burst, terminating when plasma production ends. There appears to be two sequences of positive displacement during each plasma burst: an initial acceleration at the onset of the plasma, a brief pause, and then a larger acceleration until the plasma shuts off. Such a sequence

can be considered a “Push-push” force, as there are two overall accelerations in the same direction with each voltage wave.

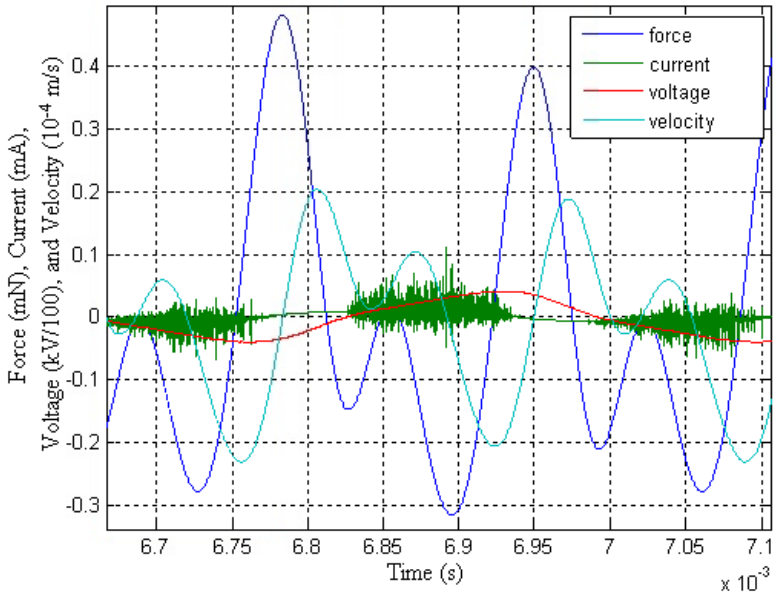

Figure 5.7. Force, plasma current, driving voltage, and actuator velocity, 8kV case

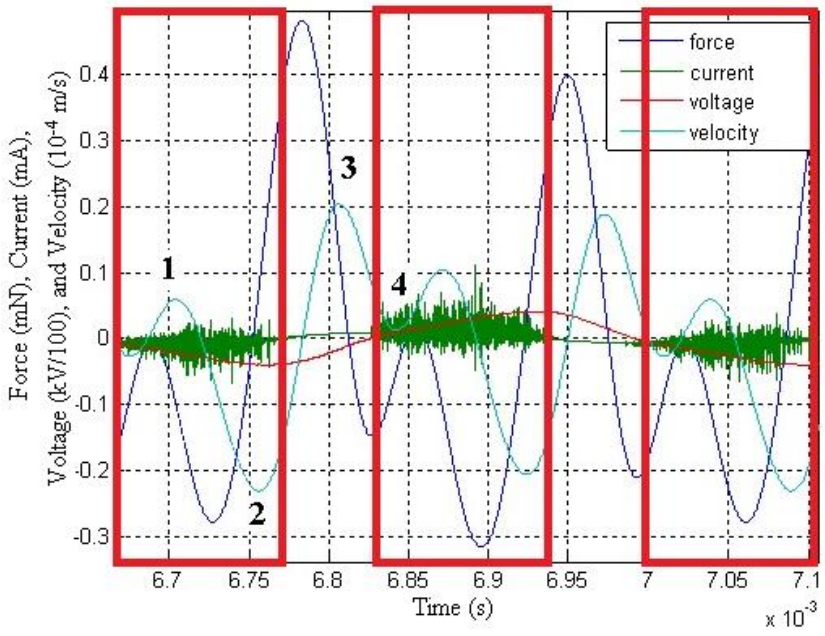

Figure 5.8. Annotated graphic of 8kV case

In Figure 5.8, locations of interest are labeled. Location 1 is a brief positive velocity that occurs at the very start of plasma generation (boxed in red) during the downward (negative-going) voltage stroke. During this time, the calculated force rises from negative 0.1mN to zero. Location 2 shows a large negative motion further into the plasma generation lifecycle. The calculated force also shows a negative trend during this time. Just before the plasma shuts off, the calculated force becomes positive and, after the plasma is quenched, the velocity becomes positive. Location 3 shows a relative maxima in both calculated force and velocity, occurring when no plasma is present. Location 4 shows the plasma cycle beginning again, this time on the positive (upstroke) cycle of voltage. The periods of positive and negative forcing and velocity are nearly identical during the upstroke and downstroke voltage cycle, with a slightly more positive

force and velocity being experienced during voltage transition from the downstroke to the upstroke (immediately after the downstroke plasma cycle).

The position data is converted to a velocity data by using MATLAB's filt-filt commands. The velocities calculated by MATLAB are time-based derivatives of position applied with a 5kHz low-pass filter. Since gravity acts as a restoring force on the freely hanging actuator, the velocity is calculated as negative when a plasma-based force is not being applied. One notable aspect of the velocity of the actuator is that the velocity values are only slightly different with the upstroke and downstroke voltage cycles. There is little difference in velocity (at most 0.05×10^{-4} m/s) depending on whether the voltage is applied positively or negatively. This is not expected, since if a large "push" were followed by a small "push" as voltage goes from negative to positive, the velocity would be unequal during each segment of the cycle. Here it is shown that since the velocities are nearly equal during the positive and negative cycles of voltage, an indication of nearly equal force is inferred.

Force reconstruction requires the use of the Fourier transform to isolate the necessary harmonic frequencies. Both displacement and phase are calculated via FFT, and then force is calculated as prescribed in chapter 3 (see equations (3.14) and (3.15)). Similar approaches were conducted for a driving voltage of 9.3kV in Figure 5.9 and Figure 5.10.

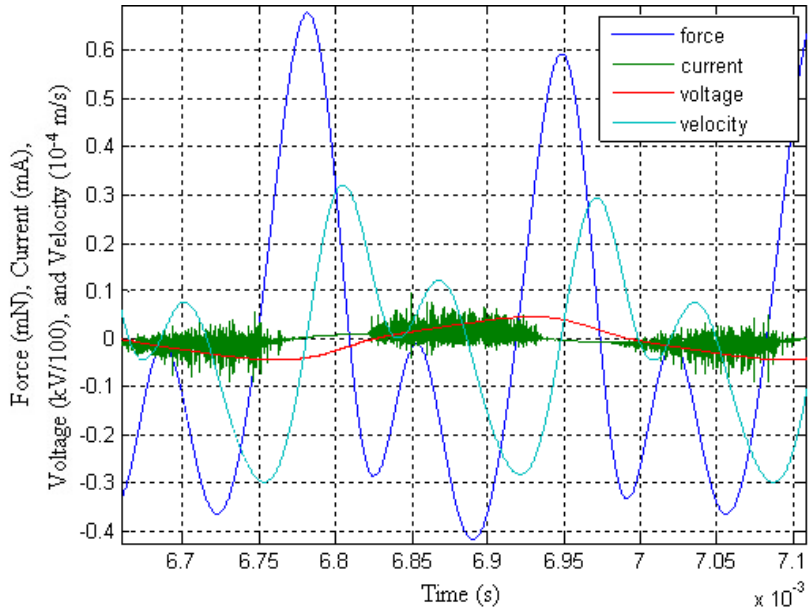

Figure 5.9. Voltage, current, filtered velocity, and computed force for 9.3kV

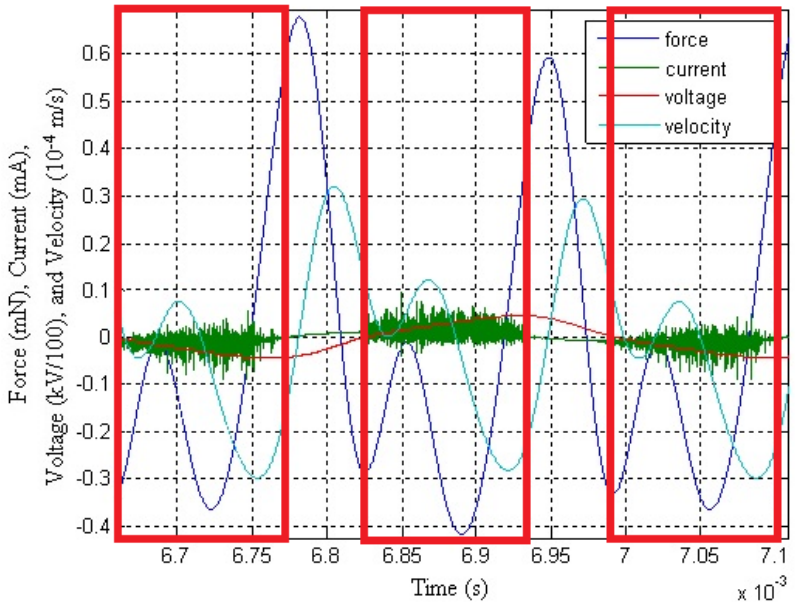

Figure 5.10. 9.3kV case with plasma generation highlighted

Figure 5.9 shows different measurements and calculated force and velocity for a 9.3kV case. The filtered velocity and resultant calculated force shows two pushes per voltage waveform: a large one at the end of each plasma burst, and a smaller force just

after the plasma begins to form. The force also experiences a slight phase shift from the acceleration. Of note are the smaller pushes that result from each plasma burst, each with small pull forces. Here one can see that there are two smaller pushes that follow each larger push, in essence, this result shows a PUSH-pull-push-pull-PUSH-pull-push-pull forcing mechanism. The cause is uncertain: experimental error may be the reason, or there may be other physical forces acting on the actuator. Further experimentation is necessary to reach further conclusion.

Other voltages show similar results. For example, a 6.5kV case is shown below in Figure 5.11 and Figure 5.12.

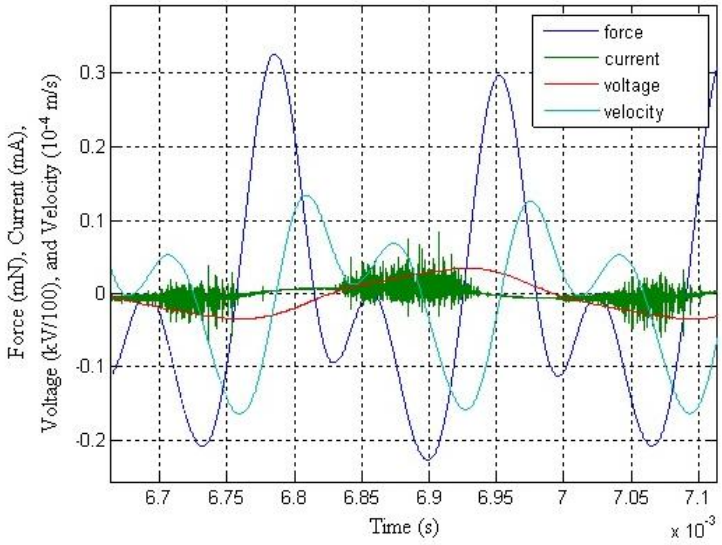

Figure 5.11. Voltage, current, filtered velocity, and calculated force for 6.5kV.

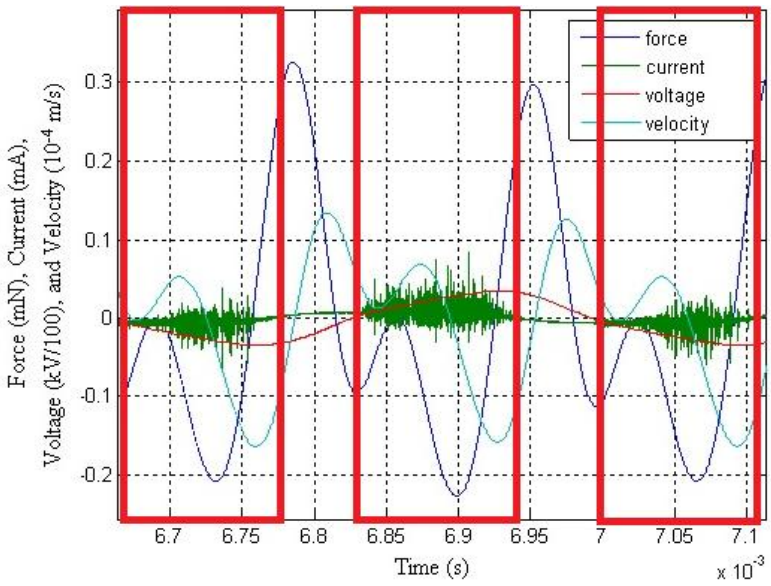

Figure 5.12. 6.5kV run with plasma generation highlighted

Clearly, the force is cut by half with only 30% reduction in voltage. One potential ramification of this may be that further large gains in force can be accomplished by smaller gains in driving voltage.

5.3. COMPARISON OF RESULTS WITH LITERATURE

Font and Enloe contend a PUSH-push [18] force with no pull force is generated by the plasma actuator, with the PUSH force dominating the forcing mechanism. Their force varied with oxygen concentration: the closest comparison to ground-level oxygen concentration they ran is 20% by volume. Their result appears in Figure 5.13 below:

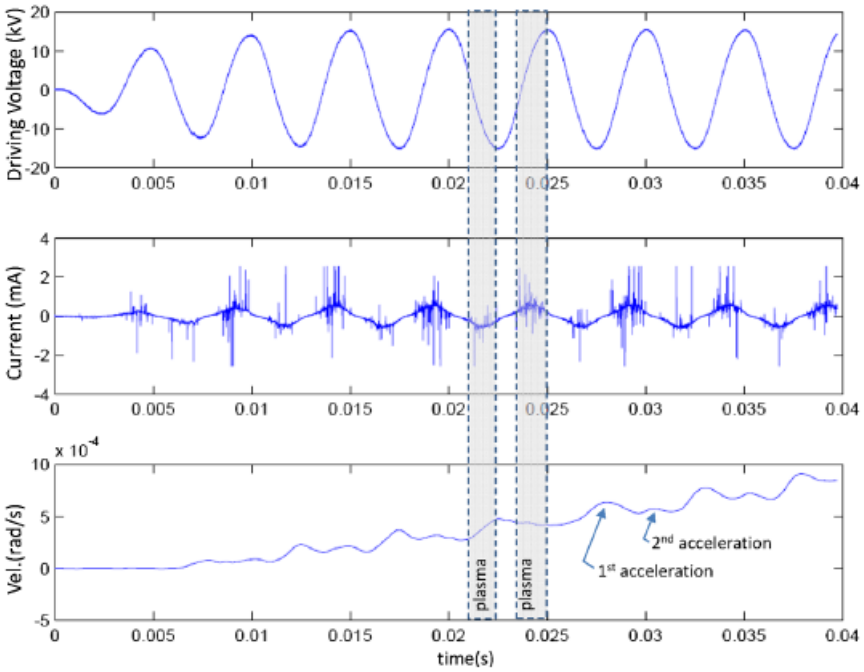

Figure 5.13. Font/Enloe plot of velocity data of an actuator at 20% oxygen (atmospheric levels)

Font and Enloe do not attempt to calculate force as it varies with time; instead, they use velocity of their apparatus to imply what the force might be. They see that the largest force is generated during the upstroke cycle of voltage. Our data shows two large PUSH forces during both the upstroke and downstroke voltage cycle.

Other methods of gathering force data are published, such as the method shown in Figure 5.14, which breaks down the plasma-induced air particle velocity into *u* and *v* components.

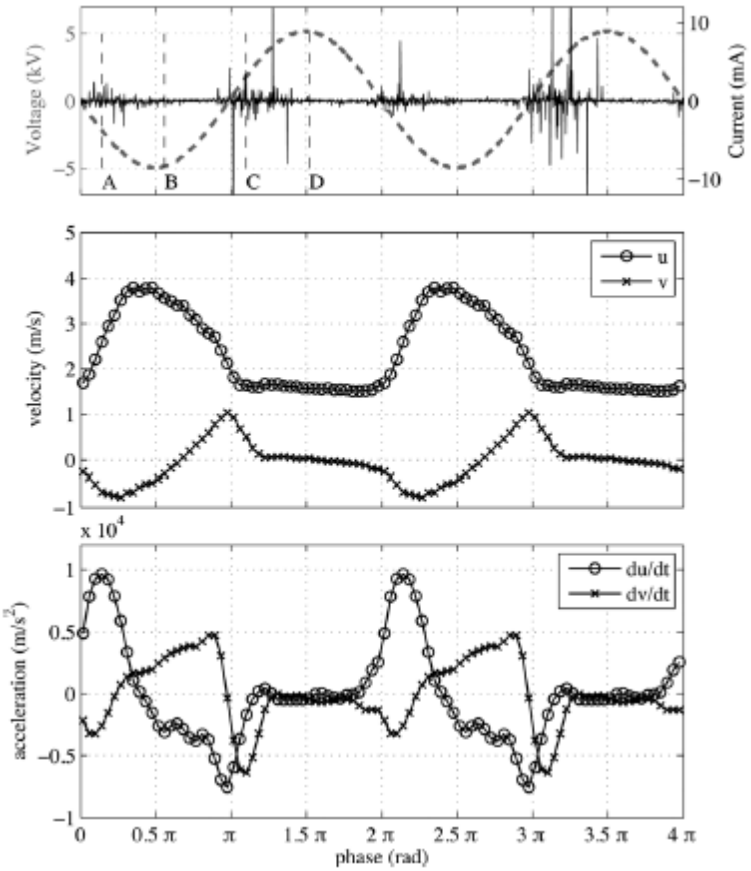

Figure 5.14. PIV measurement of particle velocity and resultant velocity and acceleration of an actuator taken by Kotsonis and Ghaemi.

Other published data concerning velocity (and inferred time-resolved force) uses optically collected data and measures departing velocity of air particles away from the plasma generation zone. Kotsonis and Ghaemi claim the initial PUSH force accounts for 90% of total force per voltage cycle. The data presented here suggests that the upstroke and downstroke forces are nearly identical in magnitude, and contain more than just two instances of forcing per voltage waveform, unlike published data.

There are large differences in published data with that presented here which can be a result of many factors. First and foremost, the actuator setup is the biggest difference. While the experiment here uses a freely hanging actuator, other published

works use secured actuators that are allowed to gyrate or pivot on a fixed arm (or not at all in cases of PIV experiments). Second, published work uses an inference of force based on detected velocity, not position, and is subject to lower sampling rates and less temporal resolution- unless low frequency voltage waveforms are used. The data presented here, displacement recorded at 100MHz at real-world application voltage frequency, represents a unique way to calculate time-varying force of a DBD actuator.

6. CONCLUSIONS

6.1. CONCLUSIONS AND RECOMMENDATION FOR FUTURE WORK

The experiment conducted here is designed to measure displacement of a DBD plasma actuator using amplification by tuned mechanical resonators, and then calculate time-varying force generated by the plasma. Designing double-clamped mechanical resonators shows that one can create a method of amplifying nanometer and sub-nanometer displacements of a body at a specific frequency. Laser interferometry advancements allow for the measurement of nanometer and sub-nanometer displacements, such as that of a plasma actuator itself. Mathematical theory, the Fourier series especially, can be used to calculate a noise-free displacement signal at specific harmonic frequencies. Finally, filtering of data and the summation of a harmonic Fourier series allows for calculation of time-varying force from a time-varying displacement.

Issues that require addressing identified throughout the course of this experiment included proper vibration isolation of the instrumentation, full grounding of all electrical systems, and methods of measuring the response of the mechanical resonators. During the course of measurement, it was discovered that slight air currents, audio pressure waves, and motion from elsewhere in the building all added to erroneous displacement measurement using a very sensitive interferometer. Great lengths concerning stabilizing the laser waveguide, laser head, and actuator mount are necessary in order to properly measure displacement. Although proper electrical grounding was attempted with all the instrumentation, there is a significant data quality improvement if a thick grounding cable tethers all components of the laser detection equipment. Finally, many different attempts at using vibrating surfaces to properly calibrate the mechanical resonators were made

before deciding on a push-pull spring-loaded solenoid configuration. If more time and budget allowed, a linear actuator or piezoelectric surface capable of high frequency motion at high precision would likely have yielded more precise control and more precise calculation of resonance of the resonator.

Future work should consist of manipulation of independent variable parameters, looking for trends, while measuring displacement and calculating velocity and force. Many parameters should be tweaked, and the effects measured, by adjusting the length of the actuator, the thickness of the dielectric barrier, and the shape, voltage, and frequency of the driving voltage waveform. Furthermore, smaller resonators designed to resonate at higher frequencies and built with different materials should be used. The use of different materials of dielectric should also be investigated. Mathematical manipulation using different filtering techniques other than the Fourier series should be investigated, in particular different cutoff frequencies and gains. Finally, the use of the actuator in different gasses and at different pressures should be attempted to identify trends in the time-varying force.

APPENDIX

```
%INTERFEROMETER OUTPUT DECODING AND GRAPHING (IODAG)
PROGRAM
%(c) 2012 Mark Emanuel, all rights reserved
%Contact the author at memanuel@hotmail.com

%Setup MATLAB for incoming data.
%Requires .csv or .xlsx file PLUS known output resolution of
%interferometer.
%clear all;
%clc;
%close all;

%Read the datafile.  Make sure you have your data file in the MATLAB
%working directory or else you must specify
%DATA = xlsread('excelfile.xlsx');
%DATA = csvread('G:\T0028ALL.csv',16,0);

%Digest datafile into time and independent 4 channel data.
%DOS command to convert files: cnvrtwfm.exe -p -l TxxxxCH*.ISF
%Set driving frequency of actuator here:
Df=3000;

Name = 'C:\Data\6_20_12\T0021CH';

DATA = csvread([Name '1.csv']);
t = DATA(:,1);  % Time data
len = length(t);% number of samples in data
A = DATA(:,2);  % A channel voltage

DATA = csvread([Name '2.csv']);
B = DATA(:,2);  % B channel voltage
DATA = csvread([Name '3.csv']);
AA = DATA(:,2);
DATA = csvread([Name '4.csv']');
BB = DATA(:,2);

A=A-B;
B=AA-BB;

Name = 'C:\Data\6_20_12B\T0008CH';
DATA = csvread([Name '3.csv']);
volt = DATA(:,2);
DATA = csvread([Name '4.csv']');
cur = DATA(:,2);
```

```
%Compute differential mode input signal using the plus/minus channels.
ASTAT=zeros(length(A),1);   % Logical value for A channel (0 or 1)
BSTAT=zeros(length(B),1);   % Logical value for B channel (0 or 1)

%CRITICAL: Set interferometer resolution ouptut in meters.
res=7.91e-2;    % nanometers per quad channel increment

%First loop: convert voltage data into pulse data of explicit binary code.

if (A(1)<0.5); ASTAT(1)=0; else; ASTAT(1)=1; end;
if (B(1)<0.5); BSTAT(1)=0; else; BSTAT(1)=1; end;
% Use hysteresis to get binary values
up = 1.5;     % Count value as a 1 if the voltage goes above 1.0V
down = -.5;   % Count value as a 0 if the voltage goes below 0.0V
for i=2:len;
   if ASTAT(i-1)==0
      if A(i)>up
         ASTAT(i)=1;
      else
         ASTAT(i)=0;
      end
   else
      if A(i)<down;
         ASTAT(i)=0;
      else
         ASTAT(i)=1;
      end
   end
   if BSTAT(i-1)==0
      if B(i)>up
         BSTAT(i)=1;
      else
         BSTAT(i)=0;
      end
   else
      if B(i)<down;
         BSTAT(i)=0;
      else
         BSTAT(i)=1;
      end
   end
end

%Initial correction for minor noise by comparing the previous, current, and
%next status for single value changes.
%for i=2:len-1;
```

```
 %   if ASTAT(i-1)==1 && ASTAT(i)==0 && ASTAT(i+1)==1
  %     ASTAT(i)=1;
   % end
   % if BSTAT(i-1)==1 && BSTAT(i)==0 && BSTAT(i+1)==1
    %    BSTAT(i)=1;
    %end
     %   if ASTAT(i-1)==0 && ASTAT(i)==1 && ASTAT(i+1)==0
     %   ASTAT(i)=0;
   %end
   % if BSTAT(i-1)==0 && BSTAT(i)==1 && BSTAT(i+1)==0
    %    BSTAT(i)=0;
   % end
%end

%Set up next loop to eliminate repeating values by looking at changes
%between A and B channels and then time-stamping the moment of change.
% time(:,1)=t(:,:);
% time(:,2)=ASTAT(:,:);
% time(:,3)=BSTAT(:,:);
% time(:,5)=A(:,:);
% time(:,6)=B(:,:);
% j=2;
skip=0;

%The "position" matrix is the ultimate output of the IODAG.  The nested
%loops first look at current status of A and B channel data.  If the proper
%channel status is met, compare with the next time step to identify if
%A-leads-B or B-leads-A in order to get the displacement change towards
%(positive) or away (negative).  Hold the time stamp value with each step
%since we need to know the time-varying displacement.
position=zeros(length(t),1);

for i=1:(length(t)-1);
    if ASTAT(i)==0 && BSTAT(i)==0
        if ASTAT(i+1)==1 && BSTAT(i+1)==0
            position(i+1)=position(i)+1;
        elseif ASTAT(i+1)==0 && BSTAT(i+1)==1
            position(i+1)=position(i)-1;
        elseif ASTAT(i+1)==1 && BSTAT(i+1)==1
            skip=[skip; i];     % INVALID CHANGE -> STORE LOCATION IN SKIP
            position(i+1)=position(i);
        else
            position(i+1)=position(i);
        end
    end
    if ASTAT(i)==1 && BSTAT(i)==0
```

```
      if ASTAT(i+1)==1 && BSTAT(i+1)==1
         position(i+1)=position(i)+1;
      elseif ASTAT(i+1)==0 && BSTAT(i+1)==0
         position(i+1)=position(i)-1;
      elseif ASTAT(i+1)==0 && BSTAT(i+1)==1
         skip=[skip; i];     % INVALID CHANGE -> STORE LOCATION IN SKIP
         position(i+1)=position(i);
      else
         position(i+1)=position(i);
      end
   end
   if ASTAT(i)==0 && BSTAT(i)==1
      if ASTAT(i+1)==0 && BSTAT(i+1)==0
         position(i+1)=position(i)+1;
      elseif ASTAT(i+1)==1 && BSTAT(i+1)==1
         position(i+1)=position(i)-1;
      elseif ASTAT(i+1)==1 && BSTAT(i+1)==0
         skip=[skip; i];     % INVALID CHANGE -> STORE LOCATION IN SKIP
         position(i+1)=position(i);
      else
         position(i+1)=position(i);
      end
   end
   if ASTAT(i)==1 && BSTAT(i)==1
      if ASTAT(i+1)==0 && BSTAT(i+1)==1
         position(i+1)=position(i)+1;
      elseif ASTAT(i+1)==1 && BSTAT(i+1)==0
         position(i+1)=position(i)-1;
      elseif ASTAT(i+1)==0 && BSTAT(i+1)==0
         skip=[skip; i];     % INVALID CHANGE -> STORE LOCATION IN SKIP
         position(i+1)=position(i);
      else
         position(i+1)=position(i);
      end
   end
end

disp(sprintf('Number of skipped data points: %i',length(skip)-1))

%Almost done.  Multiply the position displacement count by the resolution
%you input earlier.
position = position*res;

%Finally, adjust the time count since the Tektronix oscilloscope sets the
%midpoint of the data at zero seconds.  THIS MUST BE CHANGED DEPENDING ON
%THE HORIZONTAL TIME SETTING OF THE OSCILLOSCOPE DATA.  For
```

```
example, if
%computing one second's worth of data, offset the time variable by 1/2 *
%one second, or .5.  If computing 1ms of data, offset by .0005, and so on.

t = t + 0.001;

plot(t,position)
xlabel('Time (s)')
ylabel('Displacement (nm)')
title('Plasma Actuator Displacement vs. Time')
text(108,20,int2str(skip),'Fontsize',10)

voltsum(:,num)=volt;
cursum(:,num)=cur;
positionsum(:,num)=position;


%vel=zeroes(1:length(position));
%for i = 2:(length(position)-1)


%Idenfity the maximum and minimum displacement, then compute total
%deflection of the beam.

%Calculate, starting from 1ms (sample point 125001), the time needed to
% %capture a whole number of cycles and the samples required:
% period=1/Df
% cycles=floor(.009/period)
% datapoints=(len/.01)*period*cycles
% tottime=period*cycles
% datlen=length(t)
%
% len=datapoints;
% Fs=len/tottime;
% X=fft(position((datlen-(datapoints)):datlen,2),len)/len;
% f=Fs/2*linspace(0,1,len/2+1);
% XX=X(1:len/2+1);
% phase=angle(X);
% phaseX=angle(XX);
% figure; semilogy(f,4*abs(XX)); axis([0 30000 .001 500]);
% xlabel('Frequency (Hz)')
% ylabel('Magnitude (nm)')
% title('Plasma Actuator Displacement Frequency Response')
% figure; plot(f,phaseX*180/pi); axis([0 15000 -180 180])
% xlabel('Frequency (Hz)')
% ylabel('Phase (Degrees)')
```

```
% title('Plasma Actuator Phase')

% X=fft(volt((datlen-(datapoints)):datlen),len)/len;
% f=Fs/2*linspace(0,1,len/2+1);
% XX=X(1:len/2+1);
% phase=angle(X);
% phaseX=angle(XX);
% figure; semilogy(f,4*abs(XX)); axis([0 3000 min(abs(XX)) max(abs(XX))]);
% xlabel('Frequency (Hz)')
% ylabel('Magnitude (/1000V)')
% title('Input Voltage Frequency Response')
% figure; plot(f,phaseX*180/pi); axis([0 3000 -180 180])
% xlabel('Frequency (Hz)')
% ylabel('Phase (Degrees)')
% title('Input Voltage Phase')
%

% plot(t,volt,t,cur.*10,t,(position(:,2)));
% grid on;
% displ=(position(2:(length(position)),1));
% time2=(position(2:length(position),2));
%
% for i=1:datlen-1;
%     vel(i,1)=(displ(i+1)-displ(i))/Fs^-1;
% end
% for i=1:datlen-1;
%     acc(i,1)=(vel(i+1)-vel(i))/Fs^-1;
% end
% plot(time2,vel,time2,acc)
%figure; plot(t,cur)
%figure; plot(t,volt)
```

BIBLIOGRAPHY

[1] Benard, N. and Moreau, E. *Appl. Phys. Lett*., 100, 193503 (2012).

[2] Huang, J., Corke, T., Thomas, F., "Plasma Actuators for Separation Control of Low-Pressure Turbine Blades," *AIAA Journal*, Vol. 44, No. 1, pp 51-57 (2006).

[3] Poggie, J., Tilmann, C., Flick, P., Silkey, J., Osborne, B., Ervin, G., Maric, D., Mangalam, S., Mangalam, A., "Closed-Loop Stall Control on a Morphing Airfoil Using Hot-Film Sensors and DBD Actuators," 48th AIAA Aerospace Sciences Meeting Including the New Horizons Forum and Aerospace Exposition, AIAA 2010-547, Orlando, Florida (2010).

[4] Post, M., Corke, T., "Separation Control on High Angle of Attack Airfoil Using Plasma Actuators," *AIAA Journal*, Vol. 42, No. 11, pp 2177-2184 (2004).

[5] Nelson, R., Corke, T., He, C., Othman, H., Matsuno, T., Patel, M., Ng, T., "Modification of the Flow Structure over a UAV Wing for Roll Control," 45th AIAA Aerospace Sciences Meeting and Exhibit, AIAA 2007-884, Reno, Nevada (2007).

[6] Post, M., Corke, T., "Flow Control with Single Dielectric Barrier Plasma Actuators," 35th AIAA Fluid Dynamics Conference and Exhibit, AIAA 2005-4630, Toronto, Ontario, Canada (2005).

[7] Laroussi, M. "Sterilization of Contaminated Matter with an Atmospheric Pressure Plasma," *IEEE Transactions on Plasma Science*, Vol. 24, No. 3, pp 1188-1191.

[8] Roth, J. R., "Electrohydrodynamically induced airflow in a one atmosphere uniform glow discharge surface plasma," *Plasma Science,* 1998. 25th Anniversary. IEEE Conference Record - Abstracts. 1998 IEEE International, pp 291, 1-4 Jun 1998.

[9] Corke, T. C., and Matlis, E., "Phased Plasma Arrays for Unsteady Flow Control," AIAA Paper 2000-2323, Jan. 2000.

[10] Corke, T., Enloe, C., Wilkinson, S., "Dielectric Barrier Discharge Plasma Actuators for Flow Control," *Annu. Rev. Fluid Mech.*, Vol. 42, pp 505-529 (2010).

[11] Enloe, C., McLaughlin, T., VanDyken, R., Kachner, K., Jumper, E., Corke, T., "Mechanisms and Responses of a Single Dielectric Barrier Plasma Actuator: Plasma Morphology," *AIAA Journal*, Vol. 42, No. 3, pp. 589-594 (2004).

[12] Post, M., and Corke, T., "Overview of Plasma Flow Control: Concepts, Optimization, and Application," AIAA Paper 2005-0563, Jan. 2005.

[13] Corke, T. C., Post, M. L., Orlov, D. M., "Single Dielectric Barrier Discharge Plasma Enhanced Aerodynamics: Physics, Modeling, and Applications," *Review Article: Experiments in Fluids*, Center for Flow Physics and Control, University of Notre Dame.

[14] Ferry, J. W., and Rovey, J. L., "Thrust Measurement of Dielectric Barrier Discharge Plasma Actuators and Power Requirements for Aerodynamic Control," *5th Flow Control Conference*, 2010-4982 (2010).

[15] Enloe, C. L., McHarg, M. G., and McLaughlin, T. E., "Time-Correlated Force Production Measurements of the Dielectric Barrier Discharge Plasma Aerodynamic Actuator," *Journal of Applied Physics*, Vol. 103 (2008).

[16] Leonov, S., Opaits, D., Miles, R., Soloviev, V., "Time-resolved Measurements of Plasma-Induced Momentum in Air and Nitrogen Under Dielectric Barrier Discharge Actuation," *Physics of Plasmas*, No. 17 (2010).

[17] Baird, C., Enloe, C. L., McLaughlin, T. E., Baughn, J. W., "Acoustic Testing of the Dielectric Barrier Discharge (DBD) Plasma Actuator," AIAA Paper 2005–565, Jan. 2005.

[18] Font, G. I., Enloe, C. L., Newcomb, J. Y., Teague, A. L., Vasso, A. R., and McLaughlin, T. E., "Effects of Oxygen Content on the Behavior of the Dielectric Barrier Discharge Aerodynamic Plasma Actuator", AIAA Paper 2010-545, Jan. 2010.

[19] Porter, C. O., Baughn, J. W., McLaughlin, T. E., Enloe, C. L., Font, G. I., "Temporal Force Measurements on an Aerodynamic Plasma Actuator", AIAA Paper 2006-104, Jan. 2006.

[20] Durscher, R., and Roy, S., "Evaluation of Trust Measurement Techniques for Dielectric Barrier Discharge Actuators", *Experimental Fluids*, June 2012.

[21] Baughn, J.W., Porter, C.O., Peterson, B.L., McLaughlin, T.E., Enloe, C.L.,Font, G.I., Baird, C., "Momentum Transfer for an Aerodynamic Plasma Actuator with an Imposed Boundary Layer", 44th AIAA Aerospace Sciences Meeting, AIAA 2006-168 (2006).

[22] Hoskinson, A.R., Hershkowitz, N., Ashpis, D.E., "Force Measurements of Single and Double Barrier DBD Plasma Actuators in Quiescent Air". *Journal of Physics D: Applied Physics*, Vol. 41, No. 24 (2008).

[23] Kriegseis, J., Grundmann, S., Tropea, C., "Power Consumption, Discharge Capacitance and Light Emission as Measures for Thrust Production of Dielectric Barrier Discharge Plasma Actuators", *Journal of Applied Physics*, Vol. 110, No. 1 (2011).

[24] Kotsonis, M., and Ghaemi, S., "Forcing Mechanisms of Dielectric Barrier Discharge Plasma Actuators at Carrier Frequency of 625 Hz", *Journal of Applied Physics*, Vol. 110, No. 11 (2011).

[25] Mertz, B., and Corke, T., "Single-dielectric Barrier Discharge Plasma Actuator Modelling [sic] and Validation", *Journal of Fluid Mechanics*, Vol. 669 (2011).

[26] Inman, Daniel J., *Engineering Vibration*, 3rd Ed., Prentice Hall: Upper Saddle River, New Jersey (2007).

[27] http://lhotse.eng.yale.edu/wiki/uploads/3/3c/Standard_Equations.pdf

[28] Manalis, S. R., Minne, S. C., Atalar, A., and Quate, C. F., "Interdigital Cantilevers for Atomic Force Microscopy", *Applied Physics Letters*, Vol. 69, No. 25 (1996).

[29] http://www.renishaw.com/media/pdf/en/4e17f6a35a1e41d384a6b8c286802dc7.pdf

[30] Yaralioglu, G. G., Atalar, A., Manalis, S. R., Quate, C. F., "Analysis and Design of an Interdigital Canitlever as a Displacement Sensor", *Journal of Applied Physics*, Vol. 83, No. 12 (1998).

[31] http://www.physikinstrumente.com/en/products/prspecs.php?sortnr=500200

[32] White, P.J., "Design and Control of a Multi-Axis Micro-Electro-Mechanical System Array for Coordinated Micro-Manipulation," MS Thesis, Missouri University of Science & Technology (2011).

VITA

Mark D. Emanuel is a native of St. Louis, Missouri. Showing great interest in the study of meteorology at a very young age, he started a meteorology club while a student at St. Louis University High School before going on to matriculate at St. Louis University, graduating Cum Laude with a Bachelor's of Science degree in Meteorology and being awarded the James D. Collins award for most outstanding undergraduate student in the Department of Earth and Atmospheric Science.

He began his professional career working at Lambert International Airport as a weather observer/meteorological technician, later being promoted to Supervisor and then Program Manager, during a 10-year span. In 2009, he began taking engineering classes at St. Louis Community College ahead of enrolling at Missouri University of Science and Technology as a Master's student in the Department of Mechanical and Aerospace Engineering in 2010. Here, he was awarded a Chancellor's Fellowship from the University, and a Graduate Teaching Award from the Academy of Mechanical and Aerospace Engineers. Before receiving his degree in December 2012, he began his second career at a residential heating and cooling design company in St. Louis as a Project Engineer.

Mark moonlights as a volunteer radio DJ on the Pacifica Radio Network, hosting a weekly electronic dance music program that airs on FM stations nationwide, in addition to providing compelling personal interest segments for the network. He is an avid outdoorsman and enjoys hunting and golfing.